Geology, geochemistry, and geochronology of the Märjamaa rapakivi granitoid intrusion

Master's thesis

Student: Carina Potagin
Student code: 211817LARM
Supervisors: Alvar Soesoo, Professor, PhD
Juan David Solano Acosta, junior researcher
Study programme: Earth's Resources (LARM)

Tallinn 2024

Autorideklaratsioon

Kinnitan, et olen koostanud antud lõputöö iseseisvalt ning seda ei ole kellegi teise poolt varem kaitsmisele esitatud. Kõik töö koostamisel kasutatud teiste autorite tööd, olulised seisukohad, kirjandusallikatest ja mujalt pärinevad andmed on töös viidatud.

Autor: Carina Potagin
[allkiri ja kuupäev]

Töö vastab magistritööle esitatavatele nõuetele.
Juhendaja: Alvar Soesoo
[allkiri ja kuupäev]

Contents

Abstract 3
Annotatsioon 4
Figures list 5
Tables list 6
List of used terms and/or abbreviations 7
1. Introduction 8
2. Rapakivi magmatism of Fennoscandia and Estonia (European craton) 9
2.1. Svecofennian orogeny and rapakivi magmatism 9
2.3. Rapakivi characteristics 11
2.4. Rapakivi intrusions in Fennoscandia 11
3. Geology of the Estonian Precambrian basement 14
4. Material and methods 16
3.1. ICP-MS and ICP-OES analyses 16
3.2. Thin section microscopy 18
3.3. Zircon dating 18
4. Results 20
4.1. Microscopic description 20
4.2. Geochemical composition 22
4.3. Geochronology of the Märjamaa rapakivi 34
5. Discussion 35
5.1. Geochemistry and geochronology 35
5.2. Geochronology 36
5.3. Formation and geochemical features of the Märjamaa rapakivi intrusion 37
6. Conclusions 40
Acknowledgements 41
References 42
Appendix 46

Abstract

This thesis addresses the geology, geochemistry, and geochronology of the Märjamaa rapakivi granitoid intrusion using drill cores F303, F305, F306, F314, and F323. Interest towards a better characterization of Estonian geology has lately increased to obtain a more accurate picture of the economic potential of the Estonian mineral resources. The Märjamaa rapakivi intrusion lies approximately at a depth of 190-290 m and is covered by Phanerozoic sedimentary rocks. The rapakivi intrusion is characterized by its highly magnetic core.

For the study, 64 samples were collected from drill cores F303, F305, F306, F314, and F305. Out of all the samples 62 were analysed using ICP-MS to characterize the chemical variations within the intrusion. Two samples were used for U-Pb zircon dating using LA-ICPMS analysis. Additionally, seven selected samples were used for thin section microscopy to analyse the mineralogical characteristics of the rapakivi.

Based on the results, the Märjamaa rapakivi intrusion formed as a result of intraplate magmatism over the course of three intrusive phases dated back to 1629-1622 Ma. The study is the first to determine the age of the Kloostri satellite (1622 ± 4.9 Ma) considered to be the third phase of the intrusion. The Märjamaa rapakivi can be characterized as rich in rare earth elements compared to its Svecofennian counterparts, with a highly enriched interval at a depth of 290-315 m. The intrusion has also been subjected to little metasomatism due to which the geochemical composition has remained similar to its protolith. This has possibly resulted in low concentrations of Rb and Ga, and high concentrations of Ba and Sr in the Märjamaa rapakivi granite.

Märjamaa granitoidse intrusiooni geoloogia, geokeemia ja geokronoloogia

Annotatsioon

Käesolevas lõputöös käsitletakse Märjamaa rapakivi intrusiooni geoloogiat, geokeemiat ja geokronoloogiat kasutades puursüdamikke F303, F305, F306, F314 ja F323. Huvi Eesti geoloogia põhjalikuma iseloomustamise vastu on viimasel ajal suurenenud selleks, et saada täpsemat ülevaadet Eesti maavarade majanduslikust potentsiaalist. Märjamaa rapakivi intrusioon asub ligikaudu 190-290 m sügavusel ja seda katavad Fanerosoikumi settekivimid. Antud rapakivi intrusiooni iseloomustab selle väga magnetiline südamik.

Uuringu jaoks koguti 64 proovi puurdsüdamikest F303, F305, F306, F314 ja F323. Kõikidest proovidest 62 analüüsiti ICP-MS abil, et iseloomustada keemilist varieerumist intrusioonis. Kahe proovi puhul teostati U-Pb tsirkooni kristallide dateerimine, kasutades LA-ICPMS analüüsi. Lisaks valiti seitse proovi õhiku mikroskoopiliseks uuringuks rapakivi mineraloogiliste omaduste analüüsimiseks.

Tulemuste põhjal tekkis Märjamaa rapakivi intrusioon mandrisisese magmatismi tulemusena kolmes intrusiooni faasis, mille vanuseks on dateeritud 1629-1622 Ma. Uuring on esimene, mille käigus on dateeritud Kloostri satelliidi vanus (1622 ± 4,9 Ma), mida loetakse ühtlasi intrusiooni kolmandaks faasiks. Märjamaa rapakivi on rikas haruldaste muldmetallide poolest võrreldes teiste Svekofennia intrusioonidega. Eriti kõrgelt on rikastunud intervall sügavusega 290-315 m. Lisaks on intrusioon läbinud vaid kerge metasomatismi, mille tõttu on geokeemiline koostis jäänud sarnaseks tema protoliidiga. See on täenäoliselt toonud Märjamaa rapakivi graniidis kaasa madala Rb ja Ga sisalduse ning kõrge Ba ja Sr sisalduse.

Figures list

Figure 1. Crustal structure of the Svecofennian orogen as integrated across the Baltic Sea

Figure 2. Distribution of Svecofennian rapakivi complexes in space and time

Figure 3. Sketch of the Estonian crystalline basement showing the main structural zones and anorogenic intrusions

Figure 4. Map of the northwest Estonian bedrock with the Märjamaa rapakivi and placement of drill cores F303, F305, F306, F314, and F323

Figure 5. Samples being placed in a blast furnace before heating them. A Retsch jaw crusher, which was used to crush samples

Figure 6. All the prepared thin sections. A Zeiss Axioscope 40, which was used to analyse and photograph the thin sections

Figure 7. Heavy fluid separation. Zircons, which were picked for further analysis

Figure 8. Images of the Märjamaa and Kloostri rapakivi rocks, under a polarizing microscope

Figure 9. Geochemistry in the Märjamaa boreholes given as Harker diagrams. K2O (A), Al2O3 (B), TiO2 (C), Fe2O3 (D), MgO (E), MnO (F), CaO (G), and Na2O (H) (wt. %) are plotted against SiO2 (wt. %)

Figure 10. Geochemical characteristics of the Märjamaa rapakivi rocks. Chondrite normalized rare earth element diagrams (left). Additional trace elements (right)

Figure 11. Geochemical composition of the Märjamaa rocks. A) P2O5 plotted against total REE; b) Sr plotted against P2O5; c) Y plotted against P2O5; d) Zr plotted against P2O5

Figure 12. Rock classification of various diagrams

Figure 13. Geochemical classification of major elements in the rapakivi rocks of Estonia

Figure 14. Geochemical classification of major elements in the rapakivi rocks of Svecofennia

Figure 15. Geochemical classification of trace elements in the rapakivi rocks of Svecofennia

Figure 16. Geochemical classification of elements such as Sr and Ga in the rapakivi rocks of Svecofennia

Figure 17. Results from Pb/U zircon analyses by LA-ICPMS Attom method (Laser Ablation Inductively Coupled Plasma Mass Spectrometry)

Figure 18. Total REE variation in Märjamaa intrusion and its satellite in addition to Eurajoki, Kymi, Artjärvi & Sääskjärvi intrusions

Figure 19. The geochronology of rapakivis: Strömsbro, Laitila, Kloostri, Märjamaa, Ahvenisto, Wiborg

Figure 20. Outlines of magmatic intrusion phases in the Märjamaa intrusion

Figure 21. Total trace elements plotted against their measured depth from the ground

Tables list

Table 1. Major elements of the Märjamaa intrusion as arithmetic means

Table 2. Trace elements of the Märjamaa intrusion shown as arithmetic means

Table 3. Positive correlations of REEs in the Märjamaa rapakivi intrusion

List of used terms and/or abbreviations

APA – American Psychological Association

DOI – Digital Object Identifier

TalTech – Tallinn University of Technology

REE – rare earth elements

LREE – light rare earth elements

HREE – heavy rare earth elements

Ma – mega annum

Ga – giga annum

ICP-MS – inductively coupled plasma mass spectrometry

ICP-OES – Inductively Coupled Plasma Optical Emission spectroscopy

LA-ICPMS – Laser ablation inductively coupled plasma mass spectrometry

LOI – loss of ignition

MSWD –mean square of weighted deviates

1. Introduction

The post-Svecofennian A-type rapakivis typically formed between ages 1.50-1.65 Ga and are divided into four groups by age and location: Ragunda, Åland, Viborg, and Salmi intrusions (Ahl et al., 1996). Similar porphyritic rapakivi intrusions have also been found in Estonia such as the Märjamaa, Neeme, Naissaare, Ereda, and Taebla intrusions. These rapakivi intrusions have been correlated in age to the Wiborg rapakivi (Rämö et al., 1996) with the major element composition largely overlapping that of typical Finnish rapakivi granites (Kuuspalu, 1975; Kirs et al., 1991; Soesoo & Niin, 1992).

The Märjamaa rapakivi granitoid in Estonia is the result of an intraplate magmatism which formed in the crystalline basement of Estonia during the end of the Paleoproterozoic by transecting the surrounding metamorphic bedrock (Rämö et al., 1996; Soesoo & Niin, 1992). The rapakivi intrusion is covered by a sequence of Phanerozoic sedimentary rocks with a thickness varying from 190 m to 290 m since the Estonian basement dips southward (Soesoo et al., 2004; Maa-amet, 2023). The intrusion has a circular shape covering an area of ca 40 x 25 km (Soesoo & Niin, 1992). In addition to the main granitoid body, a connecting sattelite body, Kloostri, lies northwest of the intrusion covering an area of ca 10 x 12 km (Soesoo & Niin, 1992; Maa-amet, 2023).

The mineralogy and genesis of the Märjamaa rapakivi intrusion has been addressed by several studies (Kuuspalu, 1975; Kirs et al., 1991; Kivisilla, 1991; Soesoo & Niin, 1992; Soesoo, 1993; Koistinen, 1994; Rämö et al., 1996; Kirs et al., 2004). Recent studies have focused on analyzing the petrography and geochronology of the Märjamaa intrusion.

There have not been enough trace element analyses available on the Estonian rapakivi intrusions. Previously only Kivisilla (1991) and Kirs et al. (2004) analyzed trace elements within the Märjamaa intrusion using a very limited number of samples. In addition, only the main phase of the Märjamaa intrusion has been previously dated (Kirs et al., 1991; Rämö et al., 1996), with the age of other phases being unknown. Interest towards a more detailed characterization of the rapakivi intrusions has appeared due to new interest toward discovering the Estonian crystalline bedrock, regarding the new vision of the Estonian Mineral Resources until 2050 and the EU Raw Materials Initiative. The rare earth mineral concentrations within the Estonian granitoids are largely unknown and should be further analyzed.

The purpose of this study is to analyze and discuss the links and changes between geochemical, mineralogical properties, and geochronology within the Märjamaa intrusion from drill cores F323, F314, F306, F305, and F303. The center of the Märjamaa porphyritic potassium granite intrusion is highly magnetic and stands out from its Finnish and Swedish counterparts by its elevated levels of iron, magnesium, and calcium. The low silica levels in the Märjamaa intrusion compared to its Svecofennian counterparts could also result in elevated concentrations of REEs.

The information gathered by the study helps to develop a more in-depth understanding of the Märjamaa intrusion and its satellite Kloostri and to compare the trace element variations to other Svecofennian rapakivis.

2. Rapakivi magmatism of Fennoscandia and Estonia (European craton)

Rapakivi granites, first defined by Sederholm (1891) and later defined as A-type granites (Chappell, 1974; Clarke, 1992) formed due to intraplate magmatism and are an essential part of Precambrian crustal evolution on all continents (Sederholm, 1891). This thesis will focus on rapakivi magmatism of Fennoscandia and Estonia.

2.1. Svecofennian orogeny and rapakivi magmatism

The central and southern part of the Fennoscandian Shield formed as a result of the Svecofennian orogeny in the Paleoproterozoic at around 1.92-1.77 Ga in four major stages (Korja et al., 2006; Skridlaite et al., 2014) (Figure 1). Firstly, the formation of island arcs and microcontinents such as Kietele and Bergslagen which accreted to the Karelian craton (1.92-1.88 Ga) in a NW-SE trend and resulted in the formation of a large continental plate. Secondly, the newly formed continent continued with the large scale extension of the accreted crust in its southern border during 1.87-1.84 Ga. This was followed by continental collisions (1.87-1.79 Ga) with Laurentia in the NE, Amazonia in the west, Sarmatia in the SE and an unknown continent in the SW. The final stage (1.79-1.77 Ga) involved Fennoscandia undergoing a major stabilization period, with thermal collapse, thermal resetting, which was followed by granitoid magmatism and pegmatite intrusions (Korja et al., 2006).

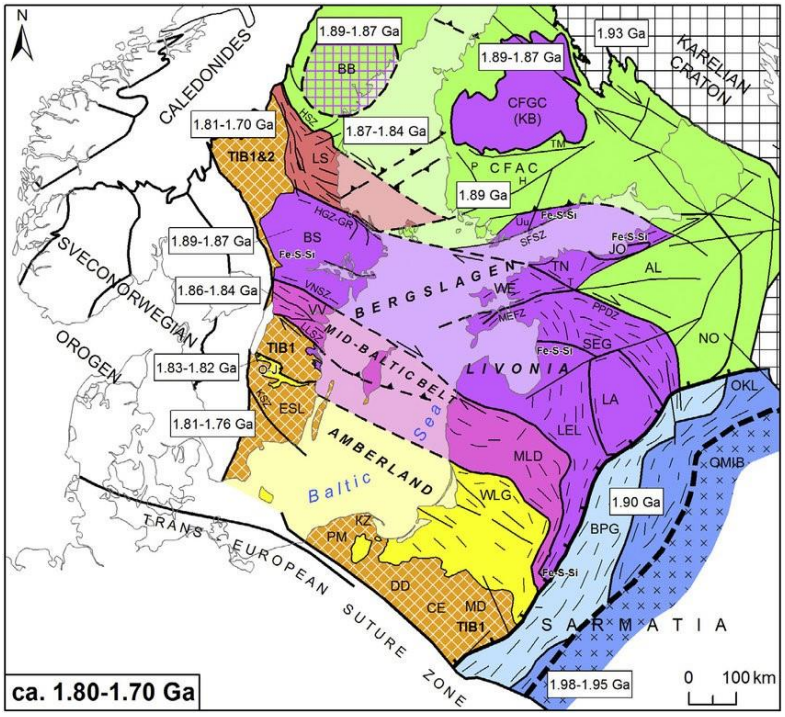

Figure 1. Crustal structure of the Svecofennian orogen as integrated across the Baltic Sea (after Bogdanova et al., 2015).

Rapakivi magmatism in the Svecofennian area formed in the aftermath of the Svecofennian orogeny at around 1.65-1.50 Ga (Ahl et al., 1996) (Figure 2). The rapakivi rocks cut through the surrounding

bedrock belonging to different lithological units which had been exposed to deformation. The intrusive rocks themselves show no internal deformation. The reason behind this intracratonic magmatism is thought to have been rift related tectonics, crustal extension and mafic underplaying at deeper levels which coincides with accretionary orogenic activity in the western part of Scandinavia (Haapala & Rämö, 1992; Elo & Korja, 1993; Korja et al., 1993; Korja & Heikkinen, 1995). This thought is also supported by the fact that the continental crust in the Fennoscandian Shield belonging to the magma provinces in Figure 2 is *ca* 50 km thick. However, the surrounding continental crust in the Svecokarelian orogen is much thicker, up to 65 km (Ripa & Stephens, 2020). The Rapakivi complexes are also located in two cross cutting belts. The longer N-S trending belt lies along the Baltic Sea from the Gulf of Bothnia to NW Lithuania The second W-E trending belt lies along the Gulf of Finland up to Lake Ladoga.

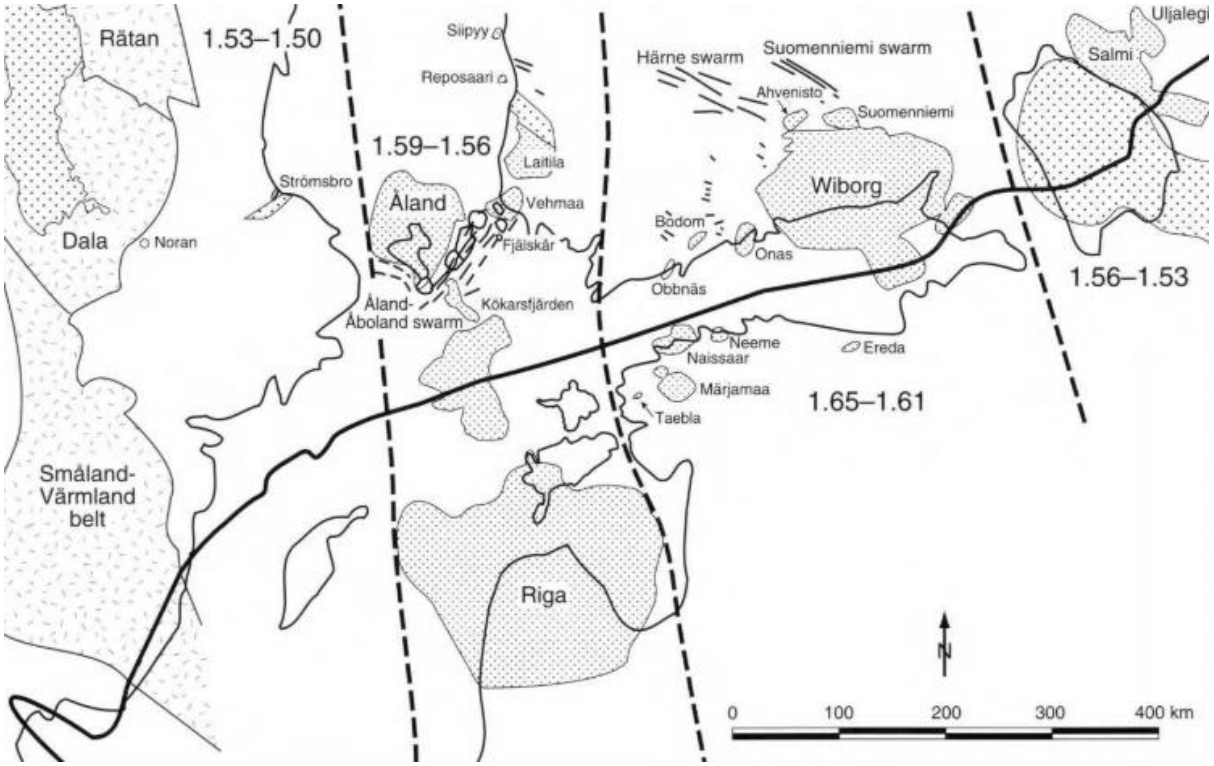

Figure 2. Distribution of Svecofennian rapakivi complexes in space and time. Densely stippled: Rapakivi complexes, lightly stippled: Jotnian sedimanetary rocks. Thick solid line marks the northern limit of the Palaeozoic platform cover rocks. The Transscandinavian Igneous Belt (TIB) is outlined in the west (after Ahl et al., 1996).

The largest rapakivi intrusions in the Fennoscandian Shield are the Riga batholith (40 000 m^3) in Estonia and Latvia, and Wiborg batholith (18 000 km^2) in Finland and Russia. Other well known rapakivi complexes in the Fennoscandian Shield are Strömsbro in Sweden, Åland, Laitila and Vehmaa in Finland, Naissaare, Märjamaa, Taebla, Neeme, and Ereda in Estonia. According to geophysical studies the Svecofennian rapakivi magmas intruded as thin sheet-like intrusions (for example, Riga batholith -5 km thick) (Elo & Korja, 1993) over a period of 20 to 60 Ma (Vigneresse, 2005).

2.3. Rapakivi characteristics

Rapakivi granites in southeastern Fennoscandia form a distinct rock group which is generally quite easy to distinguish from other granitoid rocks. The diameter of these rapakivi intrusions vary from hundreds of meters to tens of kilometres, with each having their own peculiarities in composition and/or texture.

Vorma (Vorma, 1976) characterized rapakivi texture (wiborgitic texture) as it occurs in the Fennoscandian Shield as following:

a) Ovoidal shape of the alkali feldspar megacrysts (3-4 cm and more in diameter),
b) Mantling of the ovoids by oligoclase-andesine shells (1-3 mm in thickness) some of them ovoids remaining, however unmantled,
c) Occurrence of two generations of alkali feldspar and quartz, the idiomorphic older quartz generation having crystallized as high quartz.

Rapakivi can also be described as pyterlitic, which occurs when the content of unmantled ovoids exceed that of mantled ones. However, the K-feldspar phenocrysts still have an ovoidal shape in pyterlitic rapakivi. Another common texture is porphyritic rapakivi, which describes the occurrence of angular phenocrysts in biotite granites. (Vaasjoki & Rämö, 1989)

2.4. Rapakivi intrusions in Fennoscandia

Sweden:

Strömsbro

The Stromsbrö intrusion in the eastern south-central Sweden is a small and narrow oblong rapakivi intrusion which covers an area of ca 12 km^2. The A- type granites within the intrusion are red, coarse and have a texture which is classified as intermediate between pyterlitic and porphyritic rapakivi (Vorma, 1976). The Strömsbro rapakivi contains mostly quartz, K-feldspar, plagioclase, biotite, and chlorite. The granitoid formed as a result of intraplate magmatism 1500 ± 19 Ma ago (Andersson, 1997), which makes this intrusion one of the youngest among the Fennoscandian rapakivis.

The geochemistry of the intrusion has similar characteristics to other rapakivi intrusions in the Fennoscandian Shield. The granite has a high content of trace elements such as Nb, Zr, Ga, REE, Y, Hf, Th, U, and high Fe/Mg with low Mg, Al, Ca, and P content (Andersson, 1997).

Finland:

Wiborg

The Wiborg rapakivi batholith (18 000 km^2) in south-east Finland is composed of at least four or possibly more intrusive phases (Vorma, 1971). The intrusion is characterized by its typical rapakivi texture or wiborgitic texture (Vorma, 1976). In the Finnish part of the batholith nine different rapakivi varieties have been observed: wiborgite, dark-coloured wiborgite, pyterlite, porphyritic rapakivi granite, dark-coloured rapakivi granite, even grained rapakivi granites, porphyry aplite, quartz porphyry and granite porphyry, and aplite and pegmatite (Simonen & Vorma, 1969). Most common

minerals within the intrusion are alkali feldspar, plagioclase, quartz, hornblende, and quartz with accessory minerals such as chlorite, iddingsite, and grunerite (Vorma, 1976). In addition, topaz-bearing granites have also been found within the Wiborg batholith such as in the Kymi, Artjärvi, and Sääskjärvi stocks. The Wiborg batholith is comprised of various satellites and overlapping centres of granite intrusions, such as the Ahvenisto satellite.

The Ahvenisto satellite (242 km^2) located north of the main batholith was formed by two intrusive phases. The older phase in the middle of the satellite is composed of coarse-grained biotite rapakivi and the younger phase of medium-grained hornblende rapakivi. However, unlike the in the Wiborg batholith rapakivi texture is lacking within this satellite. (Vorma, 1976)

Laitila

The Laitila rapakivi batolith (ca 1 400 km^2) in the southwest of Finland consists mainly of biotite-hornblende or biotite granite (Vorma, 1976). The granitoid is composed of reddish, homogeneous, coarse- grained, porphyritic rapakivi with feldspar megacrysts. The prevailing texture of this rapakivi can be categorized as pyterlitic with some the felspar ovoids being mantled by plagioclase rims (Vorma, 1976). The age of the first phase in the stock according to U-Pb zircon dating is 1.57 Ga (Vaasjoki, 1977). The accessory minerals are fluorite, zircon, apatite, opaque, grunerite, (and fayalite altered to iddingsite).

North of the Laitila intrusion lies the Eurajoki satellite with is composed of biotite-hornblende-fayalite granite and biotite granite. The late-stage intrusive phase of this satellite is very characteristic due to its topaz-bearing granite and cassiterite- bearing greisen veins (Haapala, 1997). The accessory minerals to this satellite are zircon, ilmenite, anatase, monazite, topaz, and cassiterite.

Estonia:

Naissaare

Naissaare is a porphyritic potassium granite intrusion covering an area of ca 35x25 km. Classical rapakivi texture has not been observed in this intrusion. The granite comprises of pink, medium- to coarse grained, microcline- megacrysts which are intersected by aplitic and microsyenitic dykes (Kuuspalu, 1975; Kirs, 1986; Soesoo & Niin, 1992). The intrusion has been dated 1.62-1.63 Ga according to U-Pb zircon dating (Rämö et al., 1996). The intrusion can be divided into two phases (Soesoo & Niin, 1992). The first phase has been observed in the periphery of the stock which has more melanocratic granites. The centre of the intrusion has been categorized as the second phase which is composed of leucocratic granites. Two generations of quartz has also been observed. Euhedral crystals within potash feldspar phenocrysts are characteristic for the first generation, whereas anhedral crystals in the groundmass are characteristic for the second generation. The additional and accessory minerals for this intrusion are epidote, fluorite, apatite, sphene, zircon, and opaques (Soesoo & Niin, 1992).

Märjamaa

Märjamaa is a porphyritic potassium granite intrusion. The rapakivi centre is highly magnetic granodioritic or quartz monzonitic, where the main mineral is hastingsitic hornblende (Kirs et al.,

2004). This phenomenon can easily be traced on magnetic anomaly maps. The SiO2 content in the central granite varies between 62-68 wt. % (Soesoo & Niin, 1992; Kivisilla et al., 1999). The central, more basic, and magnetic rock within the Märjamaa rapakivi intrusion is considered as the main phase. The magnetic core is surrounded by porphyritic hornblende-bearing biotite granite which acts as a magnetic minimum and is considered as the second phase of the intrusion (Soesoo & Niin, 1992; Soesoo, 1993). The accessory minerals such as apatite, zircon, fluorite, magnetite, titanite, and allanite have been found within the intrusion (Soesoo & Niin, 1992; Kirs et al., 1991). Rapakivi texture is lacking in the intrusion, containing mostly unmantled ovoids. The intrusion has been dated by Kirs et al. (1991) and Rämö et al. (1996), with U-Pb zircon analyses which defined the upper intercept age at 1626 ± 13 Ma and 1629 ± 7 Ma. The intrusion has a smaller satellite in its northwestern side, which is called Kloostri. This satellite, with its own magnetic minimum, has been interpreted as the third phase of the intrusion (Soesoo & Niin, 1992; Soesoo, 1993).

Neeme

Neeme porphyritic potassium rapakivi intrusion, with a diameter of ca 25 km, lies in the north of Estonia. The stock is composed of a coarse and medium grained, pinkish-grey granite in which rapakivi texture has not been observed. Instead, the prevailing texture is porphyritic rapakivi with pegmatitic structure also being observed. Only two phases have been observed within the intrusion. The main minerals within this intrusion are quartz, microcline, plagioclase, biotite, and hornblende. The additional and accessory minerals are muscovite, apatite, fluorite, sphene, orthite, zircon, and opaques. (Soesoo & Niin, 1992)

Ereda

Ereda porphyritic potassium granite intrusion has an oval shape which covers an area of ca 5x15 km. Rapakivi texture has not been observed in this intrusion. The porphyry granites are homogeneous, pinkish-grey, and coarse-grained with two generations of quartz (euhedral and anhedral crystals). Biotite granite has also been observed with some of the biotite having partly altered into chlorite. The main minerals within this intrusion are quartz, microcline, plagioclase, biotite, and hornblende. The additional and accessory minerals within the intrusion are fluorite, apatite, zircon, orthite, rutile, and opaques. (Soesoo & Niin, 1992)

Taebla

The Taebla porphyritic potassium granite intrusion covers an area of *ca* 38 km^2. It is composed of pinkish leucocratic porphyritic granites in which rapakivi texture has not been observed. Aplitic dykes cut through the granite. The main minerals within this intrusion are quartz, microcline, plagioclase, biotite, and hornblende and additional minerals are apatite, shpene, zircon, and opaque minerals (Soesoo & Niin, 1992). It has also been speculated that Taebla and Märjamaa have the same magma reservoir, where the Taebla granitoid formed as a result of the last intrusive phase similarly to the Kloostri satellite (Soesoo, 1993).

3. Geology of the Estonian Precambrian basement

Estonia is located on the southeastern slope of the Fennoscandian Shield. The crystalline basement of Estonia is Precambrian, and its surface is tilted towards the south with a decline of 0.1-0.2° - per 2.0-3.5 km (Soesoo et al., 2020). The uppermost section of the basement consists of a kaolinitic paleo-weathering crust with a thickness of up to 150 m in NE Estonia. The crystalline basement is overlain by Phanerozoic sedimentary rocks mainly from Neoproterozoic, Lower-Paleozoic, and Quaternary which have a total thickness of 100 m to 780 m. The Estonian Precambrian basement consists of metamorphic rock complexes and granitic intrusions (Figure 3).

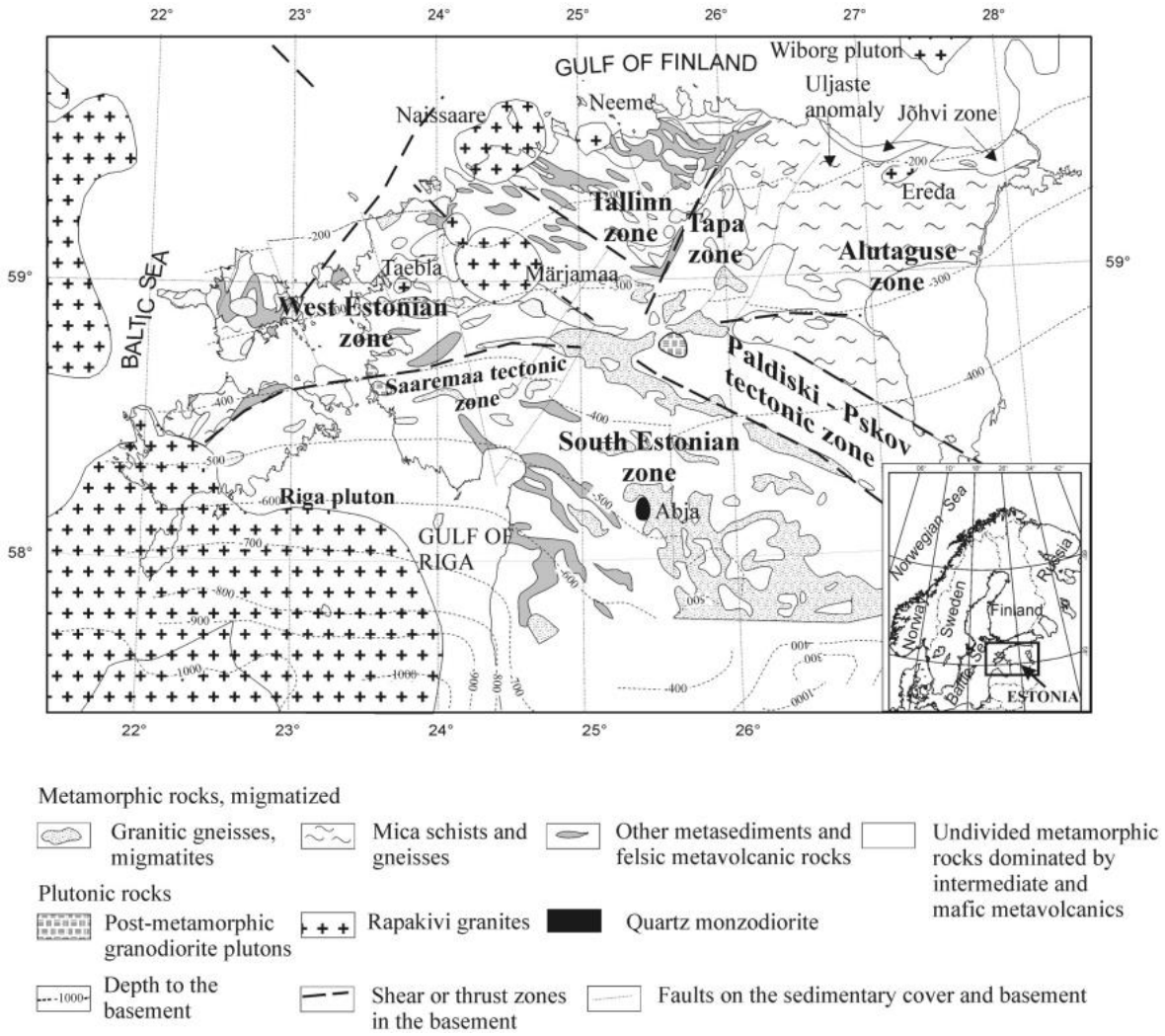

Figure 3. *Sketch of the Estonian crystalline basement showing the main structural zones and anorogenic intrusions (after Soesoo et al., 2004).*

The metamorphic rock complexes formed during the Svecofennian orogeny in 1.9-1.7 Ga as a result of an accretion of island arcs and microcontinents to the pre-existing Karelian craton (Korja et al 2006). The Estonian basement (probably except the Alutaguse zone in NE Estonia) is part of the Bergslagen region which was either a rifted continent or a back-arc region (Oen et al., 1982; Van der Velden et al., 1982). These metamorphic rocks are divided into two metamorphic faces by their metamorphic grade.

In addition, six structural-petrological zones can be distinguished which are divided by tectonic faults (Puura et al., 1983; 1997; Soesoo et al., 2004) (Figure 3). Amphibolite metamorphic faces dominate in Northern-Estonia in the Tallinn and Alutaguse zone. The Tallinn zone consists of mainly metavolcanics and-sediments while in the Alutaguse zone metapelites prevail. However, granulite faces dominate mostly in the South-Estonian zone with the smaller Tapa and Jõhvi zones located in Northern-Estonia. The South-Estonian zone is comprised of metamorphosed intermediate and mafic metavolcanics. The West-Estonian zone mainly consists of mafic amphibolite facies metavolcanics. The Precambrian bedrock of Estonia is separated by the NW-SE- striking Paldiski-Pskov tectonic fault and E-W- striking Middle-Estonian tectonic fault.

Post-Svecofennian anorogenic granite intrusions are widely distributed in the crystalline basement of Estonia with six main batoliths and intrusions: Riga, Märjamaa, Naissaare, Taebla, Ereda, and Neeme. These granitoid instrusions belong to the Fennoscandian Palaeo-Mesoproterozoic rapakivi province (Rämö & Haapala 1995; Koistinen et al., 1996; Puura & Floden, 1999) and are dated back to 1.63-1.58 Ga according to U-Pb dating (Rämö et al., 1996). Most of these intrusions mainly consist of porphyritic potassium granite apart from the largest, Riga batholith, which also comprises of gabbro-anorthosite.

4. Material and methods

Five drill cores (Adila F303; Sipa F305; Käbi F306; F314; F323) (Figure 4) from the Arbavere Research Centre were used in this thesis. These drill cores are owned by the Geological Survey of Estonia. A large portion of its geological information can be found in the database of the Estonian Land Board (https://geoportaal.maaamet.ee/est/Ruumiandmed/Geoloogilised-andmed-p115.html).

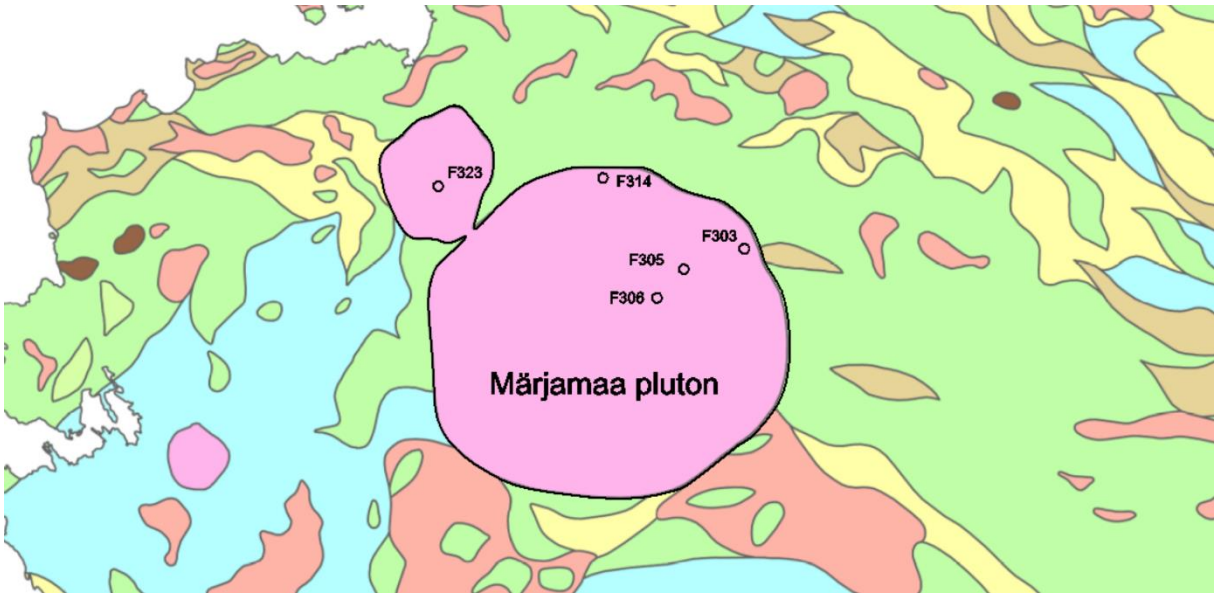

Figure 4. Map of the northwest Estonian bedrock with the Märjamaa rapakivi and placement of drill cores F303, F305, F306, F314, and F323. The bedrock map was downloaded from the Maa-amet website.

Before the sampling, I did a visual examination of the drill cores followed by photographing and creating geological descriptions of the cores. The original geological descriptions of drill cores F306 and F323 can be seen in Appendix 1 & 2. I collected samples in 2 m to 22 m intervals with the sampled sections including mostly rapakivi samples. Altogether I collected 64 from the drill cores with sample length varying between 4 cm to 18 cm (two geochronology samples were ca 30 cm). I cut all the samples along the core and sampled only half of the core. I then coded the samples and photographed them separately with a ruler for size reference.

3.1. ICP-MS and ICP-OES analyses

For 62 samples, Inductively Coupled Plasma Atomic Emission Spectroscopy and Inductively Coupled Plasma Mass Spectrometry (ICP-OES and ICP-MS) analysis was conducted. First, I crushed the bulk samples with jaw crushers and then ground them into a fine powder with a ball mill in the Institute of Geology, TalTech (Figure 5). The crushed samples were then weighed and sent to the Origin Analytical Limited laboratory in the UK for further analysis. The standard analytical protocol of the Origin Analytical laboratory for ICP-MS and ICP-OES analyses involves using a flux fusion methodology to turn samples into a liquid stage (Origin Analytical, 2024).

Figure 5. In the photo on the left samples are being placed in a blast furnace before heating the samples. In the photo on the right a Retsch jaw crusher is shown, which was used to crush the samples.

The material left over from the ICP analysis was used to determine the Loss of Ignition (LOI). For these analyses I left the samples in the drying oven overnight with the temperature set to 100°C, in order to know the sample's dry weight. When cooled and weighed, I then put the samples in a blast furnace with the temperature set to 950°C. This was necessary for me to determine the concentration of carbonates, carbon, organic matter, and volatile compounds in the samples. After drying, I weighed the samples again.

Geochemistry data from the literature

In addition, I used previously existing geochemistry data to compare Märjamaa samples to other Svecofennian rapakivi batholiths in Estonia, Finland, and Sweden. I used ninety-two geochemistry sample analyses from the Soesoo & Niin (1992) article and seventy-two samples from the Kivisilla et al. (1999) article to describe and compare chemical compositions of Estonian rapakivi intrusions. These intrusions included the major elements of Naissaare, Neeme, Ereda, and Taebla. In addition, I used analyses from the Strömsbro granite complex in Sweden. These analyses were from the Andresson (1997) article from which I only chose seven.

From Finland I used four geochemical data sets of major and trace elements to describe and compare the most notable rapakivi batholiths, such as Eurajoki and Wiborg (Kymi; Artjärvi & Sääskjärvi; Ahvenisto). For the Laittila satellite, Eurajoki in southwestern Finland, I used eight analyses from Taylor (1992) or provided by R. P. Taylor. For the Kymi stock, situated in the middle of the Wiborg batholith, I used twelve analyses from Haapala & Lukkari (2005) and Rieder et al. (1996). For Artjärvi & Sääskjärvi, in the western margin of the Wiborg batholith, I used sixteen analyses from Lukkari (2002). For the Ahvenisto satellite, northwest of the Wiborg batholith, I used five analyses given as arithmetic means from Edén (1991).

3.2. Thin section microscopy

Out of 62 samples, seven were chosen for thin section preparation. All the thin sections consisted of porphyritic potassium granite. I made the thin sections on 7.5 x 2.5 cm glass slides using the glue Petropoxy 154. After gluing a sample on a glass slide, I then cut and polished it to a thickness of 0.3 µm. I then further polished the thin section with a 2 µm grit diamond suspension for clarity. At the end of the process, I analysed and photographed the thin sections under a polarizing microscope (Figure 6). The microscope used for this process was a Zeiss Axioscope 40, which had the Axiocam 208 colour mounted on top to take photos. I made all the photos under a 2.5 x magnification objective.

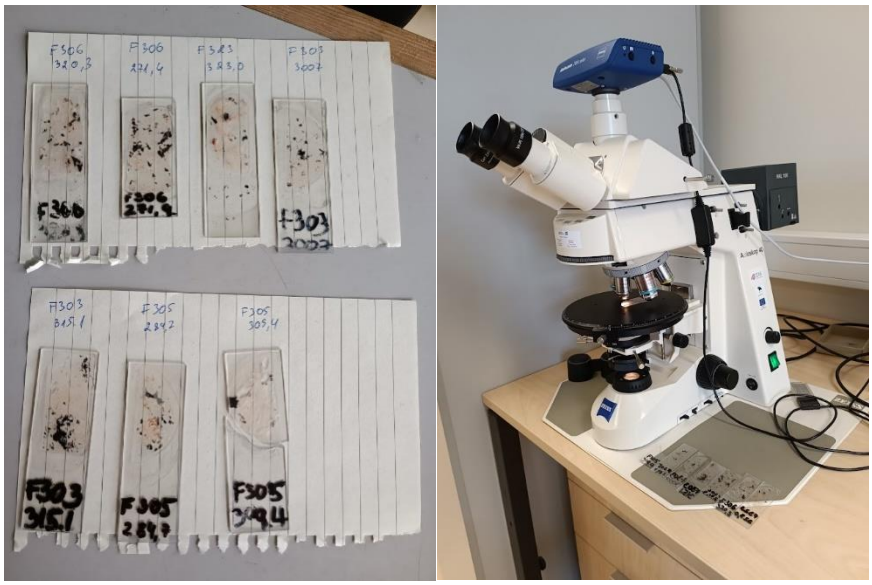

Figure 6. The photo on the left shows all the prepared thin sections. In the photo on the left a Zeiss Axioscope 40 is used to analyse and photograph the thin sections.

3.3. Zircon dating

For U-Pb zircon dating, two samples were selected, one from drill core F305 and the other from drill core F323. For this analysis 70 zircon crystals were needed for a reliable result. For the zircon separation process I first crushed and wet sieved the samples to get a crushed sample with particle size between 0.01 and 0.04 mm. I further processed the sieved samples with heavy fluid to separate heavier minerals (Figure 7). Lastly, I processed the remaining heavy minerals with magnet separation, where magnetic minerals were removed from the mass. Finally, I collected the zircons under a microscope (Figure 7). In order to verify the picked zircons, I used a scanning electron microscope. The zircon samples were then sent to the Geological Survey of Finland in Espoo for Laser Ablation Inductively Coupled Plasma Mass Spectrometry (LA-ICPMS). The U-Pb dating analyses were performed using a Nu Plasma AttoM single collector ICPMS which was connected to a Photon Machine Excite laser ablation system. The laboratory uses a calibration standard GJ-1 with an in-house reference sample A3082, and Plesovice zircon which are used in the beginning and end of each analytical session, and at regular intervals during sessions. After the analyses the data was then corrected and reduced to U-Pb isotopes ratios by calibration of concordant reference zircons (Van Achterbergh et al, 2001). In addition, common lead correction and error propagation was performed. All the ages were calculated

with 2σ errors and without decay constants errors. The $^{207}Pb/^{206}Pb$ age offset from concordant ID-TIMS ages for several samples does not exceed 0.5%.

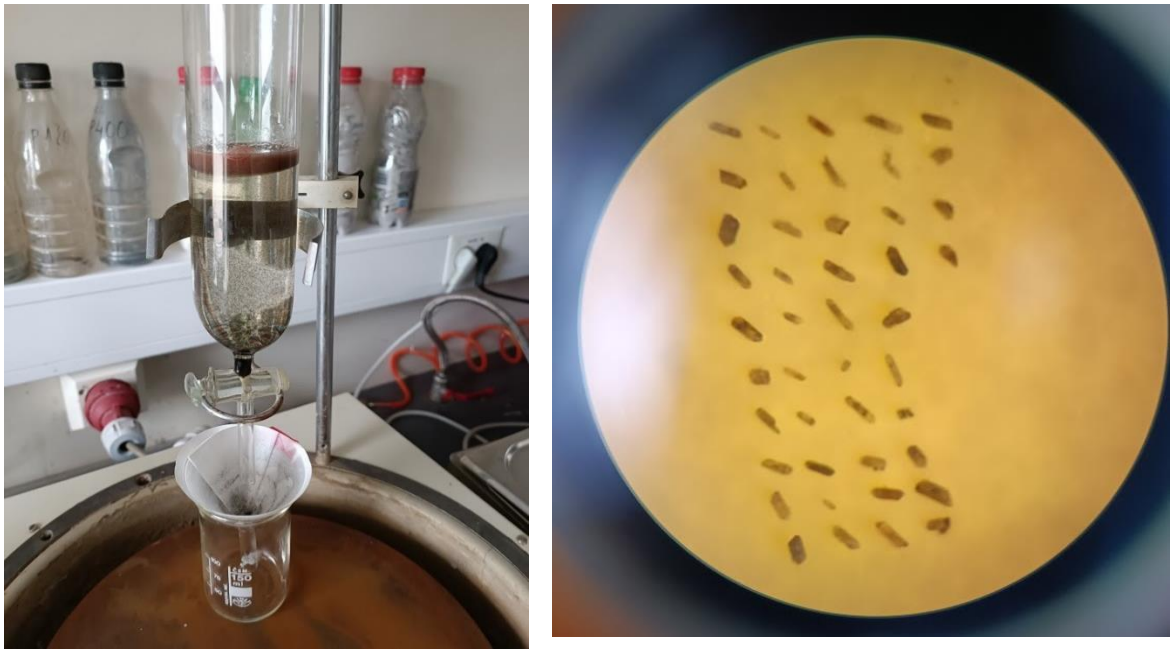

Figure 7. In the photo on the left heavy fluid separation is shown. In the photon the right zircons were picked for further analysis.

4. Results

4.1. Microscopic description

Seven thin sections from four drill cores were used to study the minerology of the Märjamaa and Kloostri rapakivi. Two thin sections were prepared from drill core F303 from depths 300.7 m (Figure 8, photos A-B) and 315.1 m (photos C-D). Two thin sections were prepared from drill core F305 from depths 284.7 m and 305.4 m (photos E and F). Another two thin sections were prepared from drill core F306 from depths 271.4 m and 320.3 m (photos G and I). The last thin section was from drill core F323 from a depth of 323.0 m.

The Märjamaa rapakivi intrusion lacks the typical rapakivi texture with plagioclase-mantled alkali feldspar ovoids. Instead, the rapakivi has porphyritic texture. Two generations of quartz crystals have previously been distinguished (Soesoo & Niin, 1992), with the first generations occurring as individual crystals and partly as inclusions within the microcline. The second generation was found occurring in the groundmass. The granites displayed slight metasomatism, in which some elements were replaced in secondary processes by other enriched elements. This has resulted in muddy textures which are especially prevalent in microcline and plagioclase. For example, in photo A sericitization of K-feldspar can be seen, where the sericitic alteration occurs in the nucleus of the crystals. This type of sericitisation can also be seen in other thin sections. However, sericitisation is usually displayed in a more scattered fashion, as is seen in other photos. In addition, fine cracks run through microcline, plagioclase, and quartz crystals.

The granites of the Märjamaa intrusion can be characterized as hornblende-biotite rapakivis, with hornblende being the more prevalent of the two. Hornblende is mostly displayed as green, varying from yellow to reddish brown. The hornblende minerals show signs of slight alterations as well, with thin cracks running through the crystals as can be seen in photo C. The accompanying biotite seems less scathed, varying from light to dark brown in coloration. Muscovite has also been found within the Märjamaa granites (Soesoo & Niin, 1992) among the second intrusive phase.

Zircon and apatite inclusions were also observed in and around biotite and hornblende crystals. These are best seen in photo C, where they occur as euhedral or subhedral grains. Apatite is displayed as small light blue elongated crystals with a length of up to 0.5 µm. These were likely formed from metasomatism induced by fluids in the protolith. Zircons exhibit birefringence with third order interference coloration under polarized light and can thus be easily identified. According to Soesoo & Niin (1992) additional accessory minerals such as fluorite, shpene, and orthite have also been noted in the Märjamaa intrusion.

Opaque minerals were also prevalent in thin sections. These are most likely represented by ilmenite, magnetite, and pyrite with varying amount titanite and allanite minerals according to Soesoo & Niin (1992) and Kirs et al. (1991). In photo C a well-developed black cubic structure can be seen which should depict a pyrite mineral. Other less developed crystals are also seen in photos E and H.

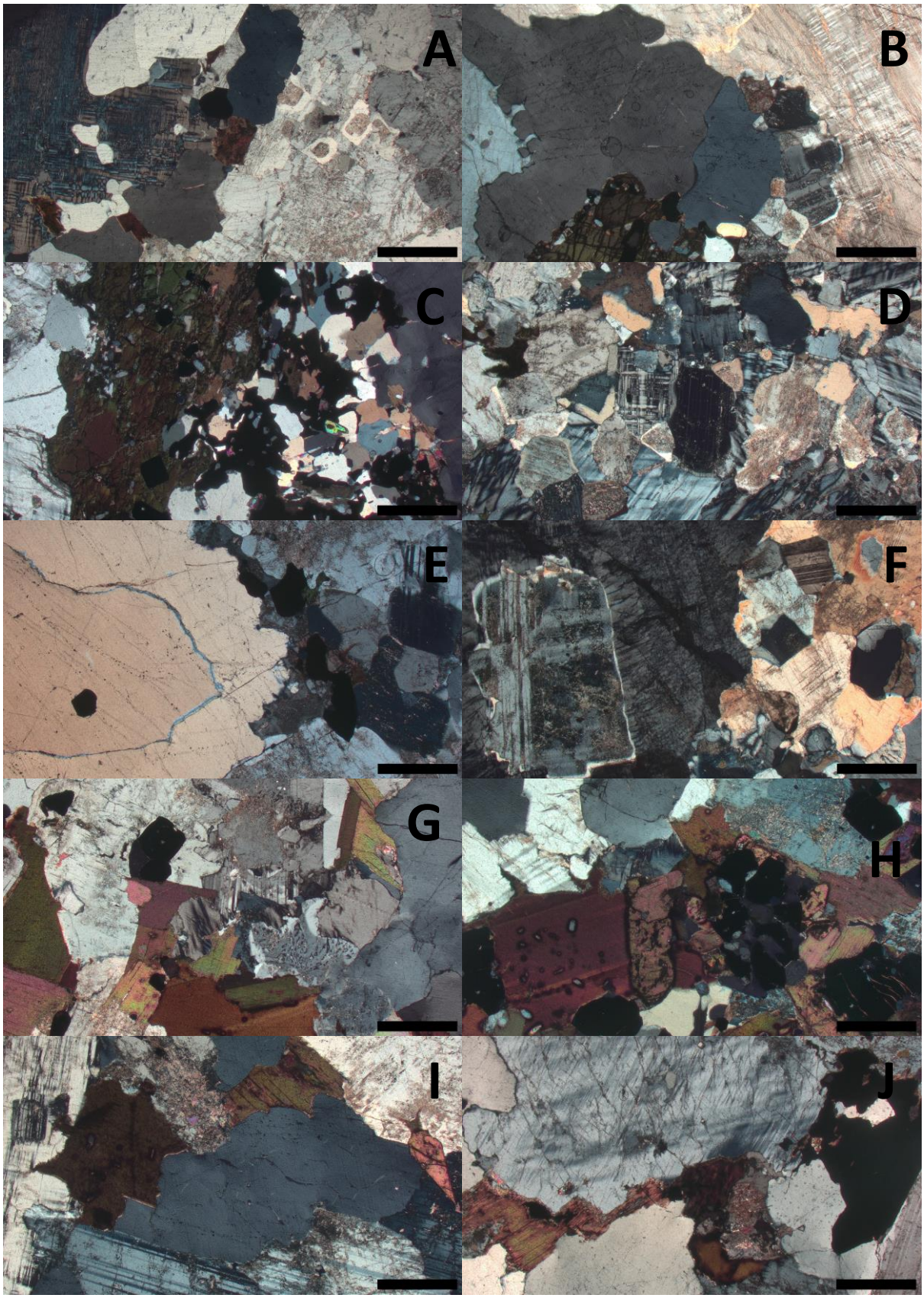
A
B
C
D
E
F
G
H
I
J

Figure 8. Images of the Märjamaa and Kloostri rapakivi rocks under a polarizing microscope. The scale bar in the corner is equal to 2 µm under the microscope. Photos A-D are from drill core F303, E-F are from drill core F305, G-I are from drill core F306, and J is from drill core F323.

4.2. Geochemical composition

Märjamaa rapakivi

Geochemical composition of the Märjamaa rapakivi intrusion has been previously analyzed by Kuuspalu (1975), Kirs (1986), Soesoo & Niin (1992), and Kivisilla et al. (1999). The previous works did not sample drill cores from Märjamaa as thoroughly and the analyses also lack trace elements. This thesis will thus concentrate on trace elements with an emphasis on REEs and their change within the Märjamaa intrusion.

Sixty-two samples from the Märjamaa intrusion were analyzed with ICP-MS and ICP-OES, of which seven are from the Kloostri satellite. These samples are reported in Table 1 as arithmetic means of drill cores F303 (16 samples), F305 (9 samples), F306 (20 samples), F314 (10 samples), F323(7 samples). In addition, F306, F305, and F323 are situated in the middle of the intrusion with F323 representing the centre of the Kloostri satellite. However, drill cores F303 and F314 are positioned in the northern edge of the intrusion, with core F314 also comprising of several intervals of gneiss.

Table 1. Major elements of the Märjamaa intrusion as arithmetic means.

Core nr		F303	F305	F306	F314	F323
SiO_2	Wt. %	65.05	67.31	64.58	69.40	70.46
TiO_2	Wt. %	0.61	0.44	0.83	0.31	0.32
Al_2O_3	Wt. %	13.85	13.13	13.38	12.66	12.61
Fe_2O_3	Wt. %	4.66	4.12	5.18	3.35	2.54
MnO	Wt. %	0.06	0.09	0.10	0.05	0.05
MgO	Wt. %	0.75	0.38	1.14	0.52	0.48
CaO	Wt. %	2.02	1.68	2.37	1.24	0.79
Na_2O	Wt. %	2.55	2.48	2.44	2.27	2.20
K_2O	Wt. %	5.49	5.87	4.98	5.61	6.17
P_2O_5	Wt. %	0.15	0.10	0.34	0.06	0.05
S	Wt. %	0.73	0.85	0.85	0.76	0.75
LOI	%	0.86	0.63	0.92	0.83	1.19
Total	Wt. %	95.20	95.59	95.34	95.47	95.67

Major elements

The recorded compositional variance ranges for the major elements in the analyzed granites were 56.86-75.34% SiO_2, 10.75-17.47% Al_2O_3, 0.14-2.01% TiO_2, 1.16-11.65% Fe_2O_3, 0.01-0.23% MnO, 0.19-2.67% MgO, 0.24-4.19% CaO, 0.20-4.49% Na_2O, 1.34-8.26% K_2O, 0.01-0.87% P_2O_5. Drill cores F323 and

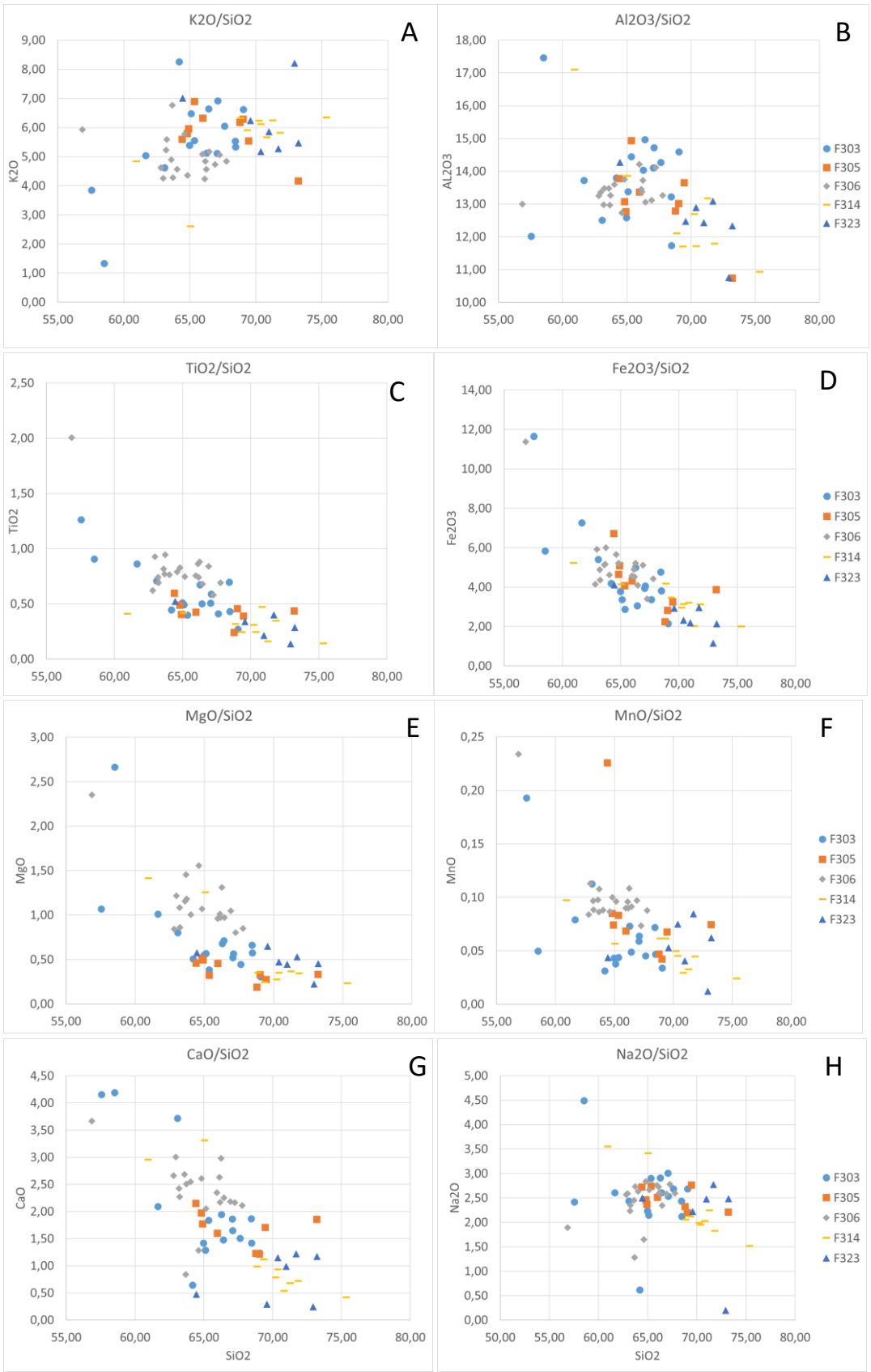

Figure 9. Geochemistry in the Märjamaa boreholes given as Harker diagrams. K_2O (A), Al_2O_3 (B), TiO_2 (C), Fe_2O_3 (D), MgO (E), MnO (F), CaO (G), and Na_2O (H) (wt. %) are plotted against SiO_2 (wt. %).

F314 stand out from having the highest average silica content (70 and 69 wt. %) with F303 and F306 having the lowest silica content (65 wt. %).

Harker variation diagrams

The data from the Märjamaa intrusion and its Kloostri sattelite are plotted as Harker variation diagrams in Figure 9. In these diagrams SiO_2 is plotted against K_2O, Al_2O_3, TiO_2, Fe_2O_3, MgO, MnO, CaO, Na_2O. The data is represented by all new 62 analyses mentioned earlier in the methods section. The data in the diagrams are colour coded with each colour representing a drill core. This makes it easier to see the differences in these drill cores and compare them.

The diagrams (Fig. 9) show a very clear trend concerning iron, magnesium, and calcium content, with an addition of titanium. Analyses poorer in silica have a higher concentration of these elements compared to those richer in silica. The lowest SiO_2 concentrations can be found in F306 followed by F303 and F305. Furthermore, drill core F303 data is the most scattered of the mentioned cores, due to the fluctuation in silica content. The highest SiO_2 concentrations can be found in cores F314 and F323, which also follow the trend by having lower quantities of iron, magnesium, titanium, and magnesium. However, magnesium concentrations have an anomaly with core F305, where the MgO content is the same or even lower than in core F314 and F323. This anomaly is also confirmed by the core average concentrations from Table 1.

A similar notable trend is also visible with Al_2O_3 and MnO, where lower silica concentrations result in higher aluminium and manganese content, such as in cores F303, F306 and F305. However, in Figure 9B the trend is indistinct among samples with silica content below 65%.

The opposite trend is normally seen in sodium and potassium concentrations, which are normally higher in more felsic rocks. In Figure 9A, this trend can be observed in potassium concentrations. There are some outliers from cores F303 and F305, which have higher potassium concentrations compared to analyses from more silica rich cores like F314 and F325. A similar trend in sodium concentrations could not be observed. The sodium concentrations seem to have no trend at all, with all cores having quite similar results.

Trace elements

Trace elements of the sixty-two analyses are presented in Table 2, where the data are presented as arithmetic means. Various diagrams were plotted using the original data, which are shown in Figures 10 & 11.

Overall, the Märjamaa intrusion analyses have elevated amounts of trace elements, especially in a certain intervall spanning from at a depth of 290-320 m. This correlation can be seen in Figure 21. The only exception being core F314, which did not have any samples at the mentioned depth. When lined up from north to south the trace element peaks are clearly visible and line up at a similar trend.

Table 2. Trace elements of the Märjamaa intrusion shown as arithmetic means.

Core nr		F303	F305	F306	F314	F323
Be	ppm	2.3	2.4	4.3	2.1	3.1
Sc	ppm	11	10	14	7.4	4.8
V	ppm	22	7.3	42.3	13	11
Cr	ppm	6.0	6.5	8.1	5.5	3.2
Co	ppm	70	85	88	86	101
Ni	ppm	5.5	6.4	6.7	5.	5.70
Cu	ppm	7.1	3.8	6.6	5.7	3.1
Zn	ppm	103	131	144	83	73
Ga	ppm	23	26	25	22	20
Rb	ppm	142	131	110	90	68
Sr	ppm	251	306	430	548	671
Y	ppm	56	82	79	51	49
Zr	ppm	680	673	817	384	444
Nb	ppm	32	38	49	31	29
Mo	ppm	2.5	4.6	4.4	1.5	1.8
Sn	ppm	1.3	1.2	2.5	1.1	1.8
Cs	ppm	0.9	1.0	1.4	0.9	1.4
Ba	ppm	1586	1695	1572	1256	1003
La	ppm	123	248	245	124	230
Ce	ppm	260	521	466	257	413
Pr	ppm	33	64	52	33	41
Nd	ppm	123	236	180	127	124
Sm	ppm	20	36	27	21	16
Eu	ppm	3.7	5.6	4.8	3.6	2.9
Gd	ppm	17	31	23	18	15
Tb	ppm	2.3	3.9	2.9	2.4	1.7
Dy	ppm	11	18	14	11	8.1
Ho	ppm	2.2	3.4	2.9	2.2	1.7
Er	ppm	5.7	8.5	7.7	5.4	4.8
Tm	ppm	0.8	1.0	1.1	0.7	0.7
Yb	ppm	4.7	6.3	7.2	4.1	4.6
Lu	ppm	0.7	0.9	1.1	0.6	0.7
Hf	ppm	15	16	19	9.6	12
Ta	ppm	1.7	1.7	2.7	1.5	2.0
W	ppm	581	745	753	779	874
Tl	ppm	0.8	0.8	1.1	1.0	1.3
Pb	ppm	27	40	39	29	38
Th	ppm	11	27	41	14	32
U	ppm	1.6	2.5	5.2	2.0	4.8

The highest concentration of trace elements (total sum, except for Ba) is in cores F305 and F306, located in the middle of the intrusion, with 3521 ppm and 3714 ppm on average, respectively. In addition, these cores also have the highest concentrations of rare earth elements (total sum) with 1265 ppm and 1113 pm. Drill core F323 located in the center of the Kloostri satellite is also rich in trace elements and REEs (3314 ppm and 913 ppm), but less compared to concentrations in the center of the main granitoid. The edge of the Märjamaa intrusion has a drastically lower concentration of these elements as is evident in cores F314 and F303.

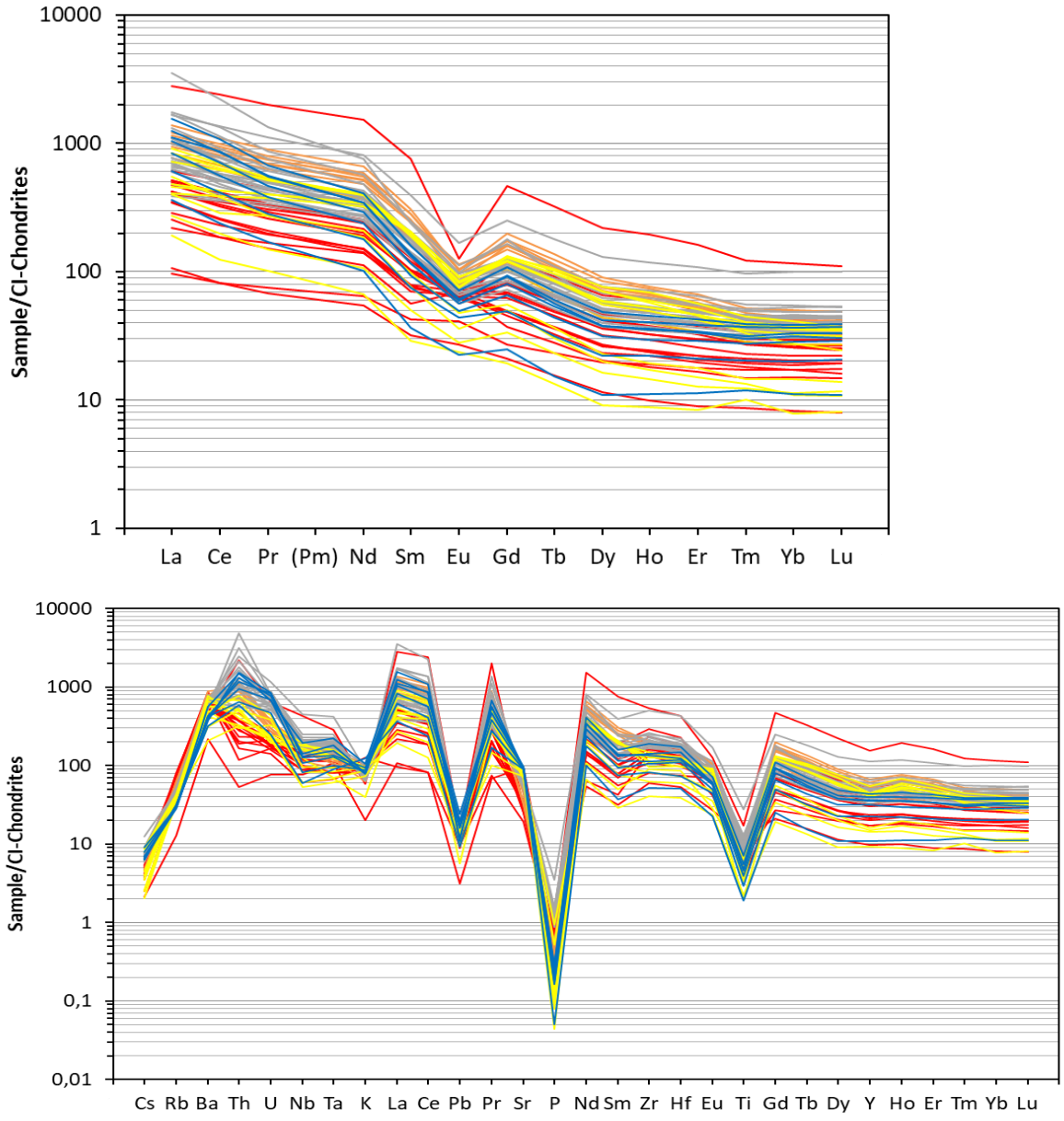

Figure 10. Geochemical characteristics of the Märjamaa rapakivi rocks. Chondrite normalized rare earth element diagrams (up). Additional trace elements (down). Each color represents a different drill core: F303-red; F305-orange; F306-gray; F314-yellow; F323-blue. Normalization after McDonough & Sun (1995).

The average of total trace elements (except Ba) in cores F314 and F303 is 2758 ppm and 2652 ppm respectively. The average of total REEs in cores F314 and F303 is 662 ppm and 664 ppm respectively.

The chondrite normalized REE and trace element diagrams in Figure 10 display the Märjamaa granitoid analyses which occur in at least two different groups (Appendix 3-12). These groups differ among light rare earth elements such as Sm, Eu, and Gd, with most having a plunging trend among these elements. However, a different group of analyses are peaking with elements Sm, Eu, and Gd.

The highest concentrations of REEs can be seen in drill core F303 in the highly enriched interval which lies at a depth of 299 m. The REE concentration in this sample was 3604 ppm making it over five times higher than the drill core average. Elements with the highest concentrations in the sample were among the LREEs with Ce (1468 ppm), La (665 ppm), and Nb (700 ppm) having the highest content. These elements have higher concentrations in other samples as well compared to HREEs. Another highly enriched sample is in drill core F306 at a depth of 311 m, however it has lower REE content compared to drill core F303.

HREEs mostly have concentrations under 5 ppm with the exception of Dy (mostly 4-22 ppm, in F303 up to 54 ppm) and Er (1-11 ppm, in F303 up to 25 ppm). In addition, Y also has rather high concentrations ranging from 15-244 ppm. The HREEs are all in strong positive correlation with each other (Appendix 13).

The LREEs are also in positive correlation to each other, however it is weakest among elements such as La, Ce, and Eu (Appendix 13). As mentioned before, Ce, La, and Nd have the highest concentrations in the Märjamaa intrusion among all the REEs. The content of Ce in samples ranges between 50-1468 ppm with the average being 381 ppm. The content of La in samples ranges between 22-838 ppm, with the average being 193 ppm and the content of Nd ranges between 25-700 ppm, with an average of 158 ppm.

There was positive correlation between REEs and trace elements such as Sc, Zn, Nb, Ga, Y, and Zr in the Märjamaa intrusion (Appendix 14 & 15). In addition, there was also positive correlation between major elements and REEs, such as Fe, Ti, Mn, Ca, however the correlation was much weaker compared to the mentioned trace elements. Furthermore, there was no correlation between REEs and the following elements: Si, Na, Ka, Rb, Sr, and Ba.

Even more fractionations can be seen in diagram Figure 10b, most notably among elements Th, U, Nb, and Ta. Uranium and thorium have elevated concentrations in cores F306 and F323 with Nb and Ta also being enriched in core F306. Table 2 also shows elevated values of vanadium in core F306 at four times the average of the Märjamaa samples, especially compared to more felsic samples. In addition, samples poorer in silica had higher concentrations of Mo, Rb, Zr, and Ba. However, samples richer in silica had higher values of Sr and W.

Grouping of samples

Samples from the Märjamaa intrusion show clear grouping when plotting trace elements against P_2O_5. Some of the most notable examples are shown in Figure 11. It was previously pointed out that the total rare earth elements appear to be highest in more basic samples. In Figure 11A another pattern

can be observed, where two different clusters of samples emerge when plotting P_2O_5 against total REEs. In the first group, cores F305, F314, and F323 form a trend, where the rise in total REEs results in a slight rise in phosphorus content. In the second group, the rise in total REEs is followed by a much more drastic increase in phosphorus content. A similar grouping can also be seen in Figure 11C and 11D where P_2O_5 is plotted against yttrium and zirconium. However, in Figure 11D the grouping is less clear, due to the fact that the analyses from core F303 are more scattered.

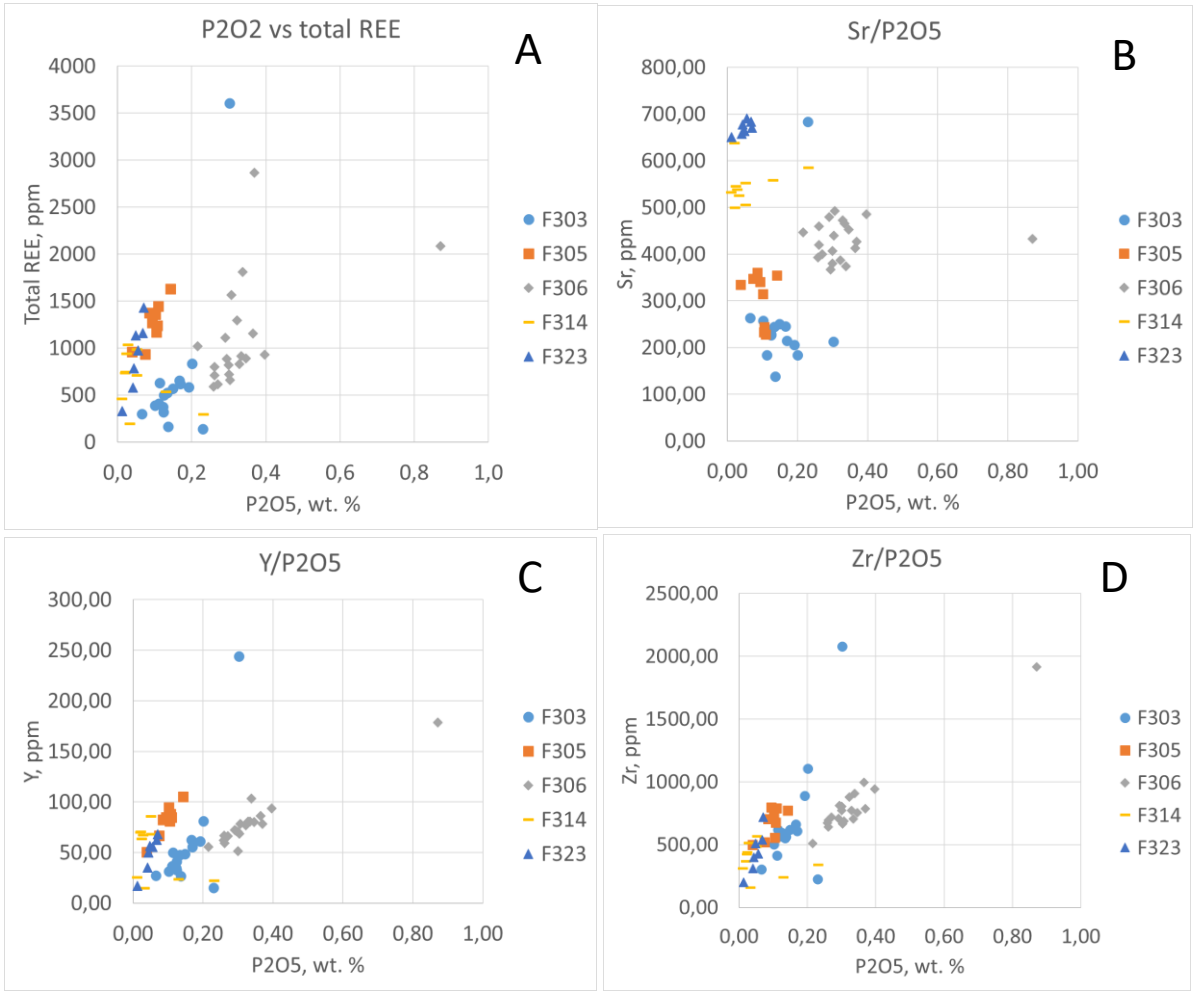

Figure 11. Geochemical composition of the Märjamaa rocks. A) P_2O_5 plotted against total REE; b) Sr plotted against P_2O_5; c) Y plotted against P_2O_5; d) Zr plotted against P_2O_5.

An interesting grouping can also be observed in Figure 11B, where strontium is plotted against P2O5. Strontium concentrations seem to be different in all the analyzed cores, which form completely independent clusters when plotted against phosphorus. It is also notable that the strontium levels in each drill core remain similar despite the change in silica concentrations.

Classification of the Märjamaa rocks

Geochemically, rapakivi granites from the Märjamaa intrusion and its Kloostri satellite are alkaline or slightly high-K calc – alkaline (Figure 12A). They can also be categorized as ferroan with high ratios of FeO/(MgO+FeO). It is even possible to see stratification of samples by cores in the ferroan diagram in

Figure 12C, with cores F305 and F314 having the highest concentrations in FeO/(MgO+FeO) ratios, followed by cores F303, F323, and F306. In general, the alkaline and ferroan properties of the Märjamaa and Kloostri intrusions are also typical to the Finnish rapakivi granites.

Rapakivi rocks are normally identified as A-type granites which formed due to intra plate magmatism. Figure 12C confirms that samples from the Märjamaa intrusion do indeed fall into that classification, with some exceptions. The Märjamaa samples tilt towards the volcanic arc granites classification according to the tectonomagmatic diagram in Figure 12D. However, some Finnish rapakivi granites tend to slightly tilt into the category of syn collision granites (Rämö & Haapala, 1995).

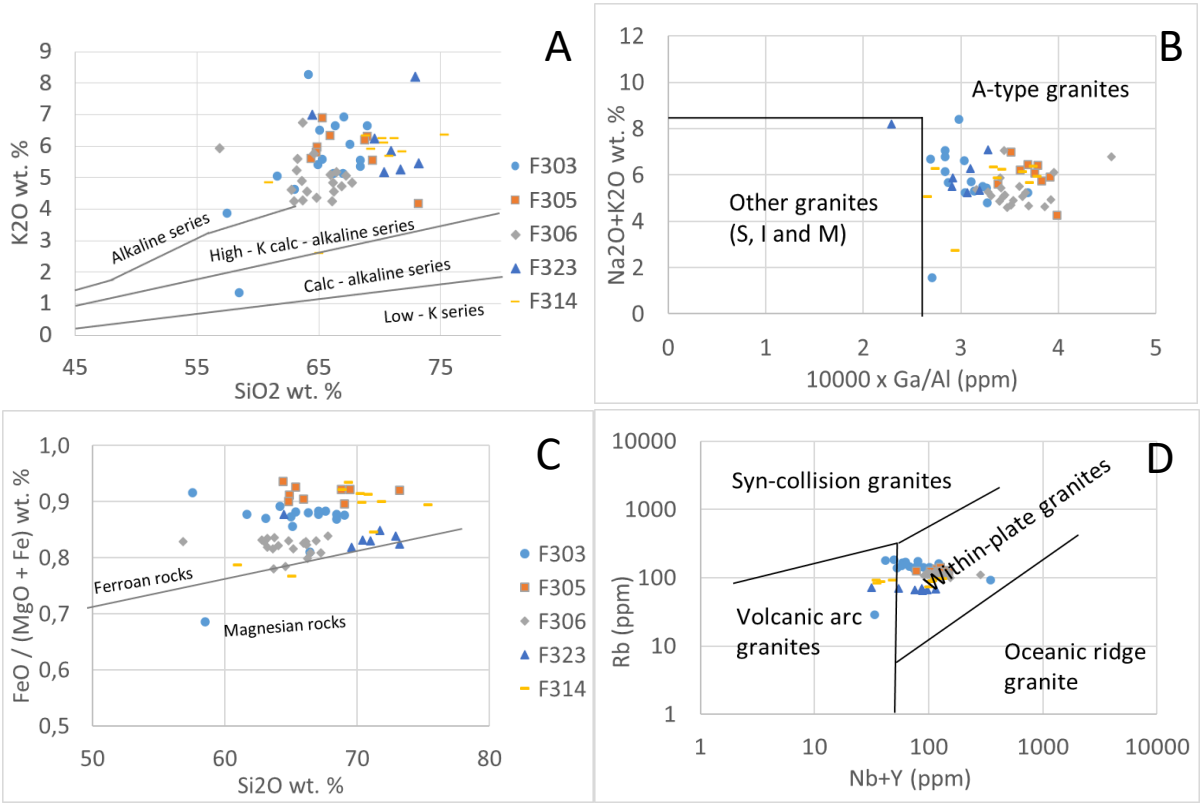

Figure 12. Rock classification of various diagrams. A) Compositional classification of rocks from alkaline to low-K series (Ewart, 1982); B) ferroan-magnesian rock classification (Frost & Frost, 2008); C) Classification of A-type granites (Whalen et al., 1987); D) tectonic interpretation of granitic rocks (Pearce et al., 1984).

The Estonian rapakivi intrusions

Some of the major elements in the Estonian rapakivi intrusions were compared in Figure 13, which included Märjamaa and its satellite Kloostri in addition to Neeme, Naissaare, Ereda, and Taebla intrusions. The major elements used in Figure 13 are Na_2O, MgO, CaO, and K_2O which were plotted against SiO_2. No trace elements were compared due to the lack of trace element analyses among other Estonian rapakivi intrusions.

The silica concentrations in the Märjamaa intrusion vary the most out of all the Estonian rapakivi intrusions. Silica content in the Naissaare and Neeme intrusions in addition to the Kloostri satellite also vary significantly with Naissaare being slightly more basic (60-72 wt. %) compared to others. Since the Ereda and Taebla intrusions had the least number of analyses, the elemental concentrations are less variable, and are thus shown only to depict an approximation of an intrusion.

The MgO concentrations have the most overlapping among the rapakivi samples compared to other diagrams, especially among Mg concentrations in an interval of 0.2-1.0 wt. %. The Märjamaa intrusion had the highest magnesium content followed by Neeme. This shows a clear correlation between high MgO and low SiO2 content. The Naissaare intrusion and Kloostri satellite analyses show a less clear correlation between these elements.

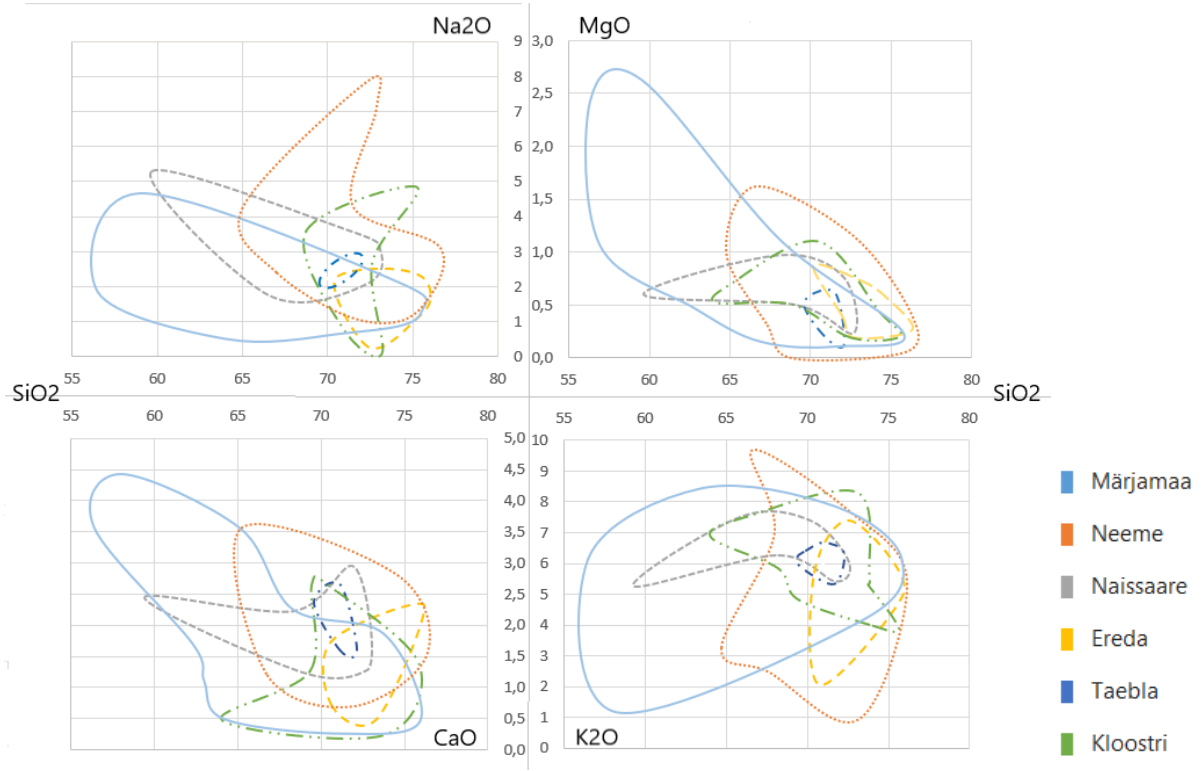

Figure 13. Geochemical classification of rapakivi rocks in Estonia: Märjamaa (light blue), Neeme (orange), Naissaare (grey), Ereda (yellow), Taebla (dark blue), and Kloostri (green). A) Na_2O plotted against SiO_2, B) MgO plotted against SiO_2; C) CaO plotted against SiO_2, D) K_2O plotted against SiO_2. All figures are shown as wt. %. Analyses of Neeme, Naissaare, Ereda, and Taebla intrusions are from Soesoo & Niin (1992) and Kivisilla et al. (1999).

The Märjamaa and Ereda intrusions have the lowest concentrations of Na_2O, followed by Naissaare. However, Kloostri and Neeme samples have the most varied content of Na_2O with Neeme reaching close to 8 wt. %. These high peaks are mostly single exceptions. Many of the analyses follow a similar trend to Märjamaa and Naissaare intrusions where lower silica content has higher Na_2O concentrations.

The most overlapping among CaO concentrations in Figure 13 happens around 1.5-2.5 wt. %. Märjamaa and Kloostri have the lowest concentrations of CaO (below 0.5 wt. %) among Estonian rapakivis with Märjamaa also having the highest values. CaO concentrations also vary significantly in the Neeme intrusion, which peaks with 3.5 wt. %.

The average concentration of K_2O among Estonian rapakivi intrusions is around 5-8 wt. %. The Märjamaa, Neeme, and Ereda intrusions have samples with the lowest K_2O content, with Neeme also having the highest concentrations of up to 9.5 wt. %.

Svecofennian rapakivi intrusions

Some of the major elements of Svecofennian rapakivi intrusions were compared in Figure 14 including Märjamaa, Eurajoki, Kymi, Artjärvi and Sääskjärvi, Ahvenisto, and Strömsbro stocks. These major elements are Na2O, MgO, CaO, and K_2O which were plotted against SiO_2. The analyses results from Finnish and Swedish rapakivis were given as drill core averages.

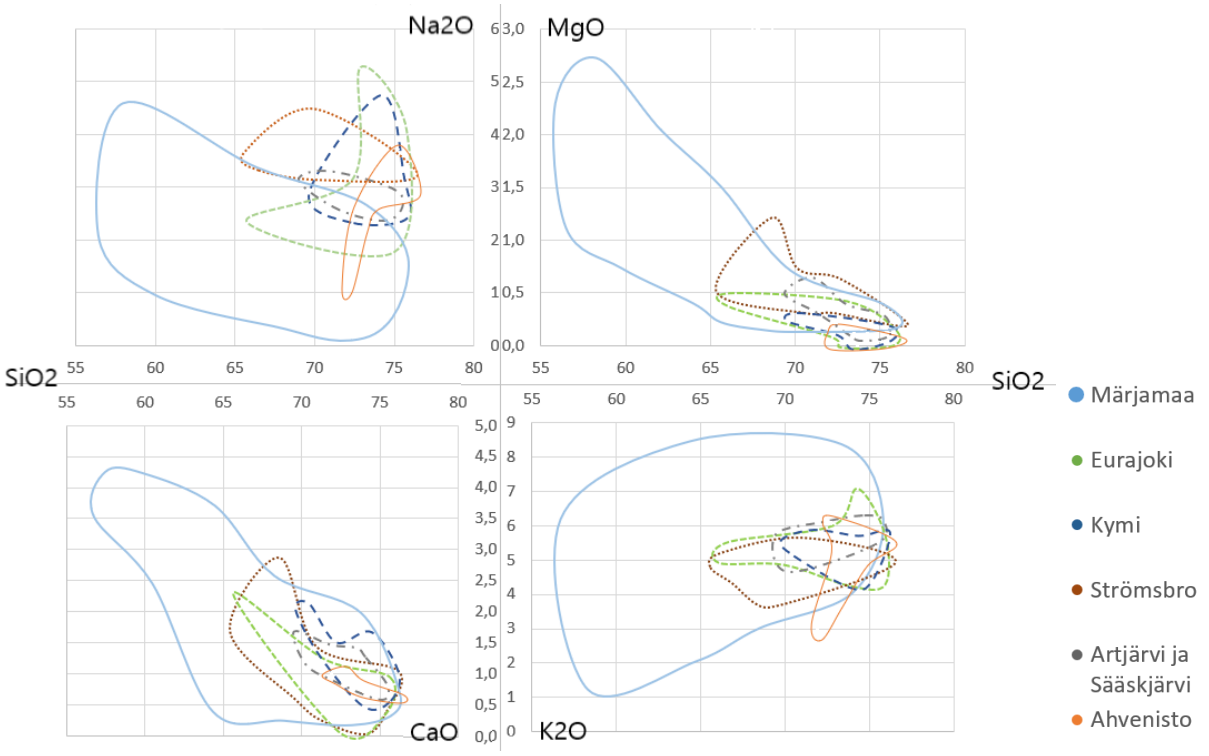

Figure 14. Geochemical classification of rapakivi rocks in Svecofennia: Märjamaa (light blue), Eurajoki (green), Kymi (dark blue), Strömsbro (dark red), Artjärvi & Sääskjärvi (purple), and Ahvenisto (orange). A) Na_2O plotted against SiO_2, B) MgO plotted against SiO_2; C) CaO plotted against SiO_2, D) K_2O plotted against SiO_2. All figures are shown as wt. %. Analyses of Strömsbro are from Andresson (1997), Ahvenisto form Edén (1991), Artjärvi & Sääskijärvi from Lukkari (2002), Kymi from Haapala & Lukkari (2005) and Reider et al. (1996), Eurajoki from Taylor (1992) or provided by R. P. Taylor.

The Finnish and Swedish rapakivis are more silica rich than the Märjamaa intrusion where granite's averages vary from 64-70 wt. %. The higher silica concentrations also result in differing results of other major elements and the biggest disparity of this can be seen when comparing MgO concentrations. In Finnish and Swedish rapakivis MgO content varies between 0.1-1 wt. %, whereas

in the Märjamaa intrusion it peaks at 2.7 wt. %. Among Svecofennian rapakivis Ahvenisto and Kymi have the lowest average MgO content followed by Eurajoki.

Concentrations of Na_2O among Finnish and Swedish analyses are also higher on average (between 2-4 wt. %) compared to Märjamaa when looking at Figure 14. However, when comparing the drill core averages (Table 1) of the Märjamaa intrusion, Na2O content results fall into a similar range (2.20-2.55 wt. %) with others.

Calcium concentrations vary significantly in Märjamaa, similarly to MgO concentrations, due to the variation in silica. Other Fennoscandian rapakivis have on average MgO concentrations between 0.5-2.0 wt. %, however MgO concentrations in Märjamaa can reach close to 4.5 wt. % among the most basic rocks.

In addition, the Märjamaa intrusion also has the most varying K20 concentrations (1.0-8.5 wt. %), with the drill core averages being (4.98-6.17 wt. %). The drill core averages of the Märjamaa intrusion are more similar in range to the other Svecofennian results which on average vary between 4-6.5 wt. %.

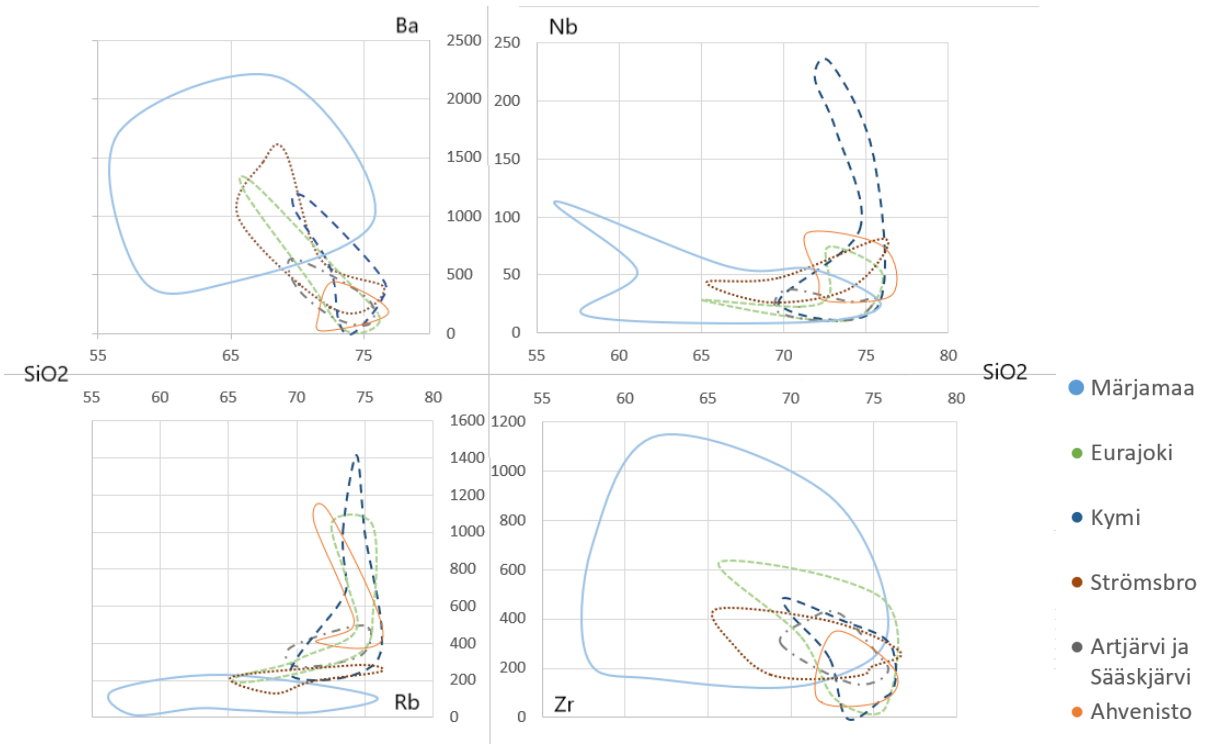

Figure 15. Geochemical classification of rapakivi rocks in Svecofennia: Märjamaa (light blue), Eurajoki (green), Kymi (drak blue), Strömsbro (dark red), Artjärvi and Sääskjärvi (purple), and Ahvenisto (orange). A) Ba plotted against SiO_2, B) Nb plotted against SiO_2; C) Rb plotted against SiO_2, D) Zr plotted against SiO_2. SiO_2 is displayed as wt. % and Ba, Nb, Rb, and Zr are displayed as ppm. Analyses of Strömsbro are from Andresson (1997), Ahvenisto form Edén (1991), Artjärvi & Sääskjärvi from Lukkari (2002), Kymi from Haapala & Lukkari (2005) and Reider et al. (1996), Eurajoki from Taylor (1992) or provided by R. P. Taylor.

Some of the trace elements of Svecofennian rapakivi intrusions were also compared in Figure 15. These trace elements are Ba, Nb, Rb, and Zr which were plotted against SiO_2. The analyses results from Finnish and Swedish rapakivis were mostly given as drill core averages.

The Märjamaa intrusion has slightly higher Ba concentrations than in other Svecofennian intrusions with the drill core averages in Märjamaa varying between 1000-1700 ppm. The most similar rapakivis in comparison are Strömsbro, Eurajoki, and Kymi, which have the highest Ba concentrations (ca 100-1500 ppm) compared to others. However, Artjärvi & Sääskjärvi, and Ahvenisto stocks have much lower average Ba concentrations reaching only up to ca 500 ppm.

Niobium concentrations are similar in most rapakivis as seen in Figure 15, with average concentrations between 25-75 ppm. However, Kymi stock has very high peaks of Nb concentrations reaching *ca* 225 ppm, which is characteristic to topaz bearing granite. In addition, the Artjärvi & Sääskjärvi stock has slightly lower concentrations of Nb varying between 13-31 ppm.

The Märjamaa intrusion has very low concentrations of rubidium with the borehole averages varying between 65-150 ppm. This is similar to the Strömsbro intrusion followed by the Artjärvi & Sääskjärvi stock which also has low rubidium values. Ahvenisto, Kymi, and Eurajoki stocks have varying Rb concentrations ranging between 200-1200 ppm, with Kymi peaking at ca 1400 ppm.

The zirconium content in the Märjamaa intrusion is slightly higher than in other Svecofennian rapakivis with the drill core averages ranging between 383-817 ppm. The Finnish and Swedish stocks overlap at concentrations between 400-200 ppm. The Ahvenisto stock has the lowest average zirconium content out of all the stocks. However, Eurajoki has the most varying analyses results out of the Finnish and Swedish rapakivis ranging between 30-619 ppm.

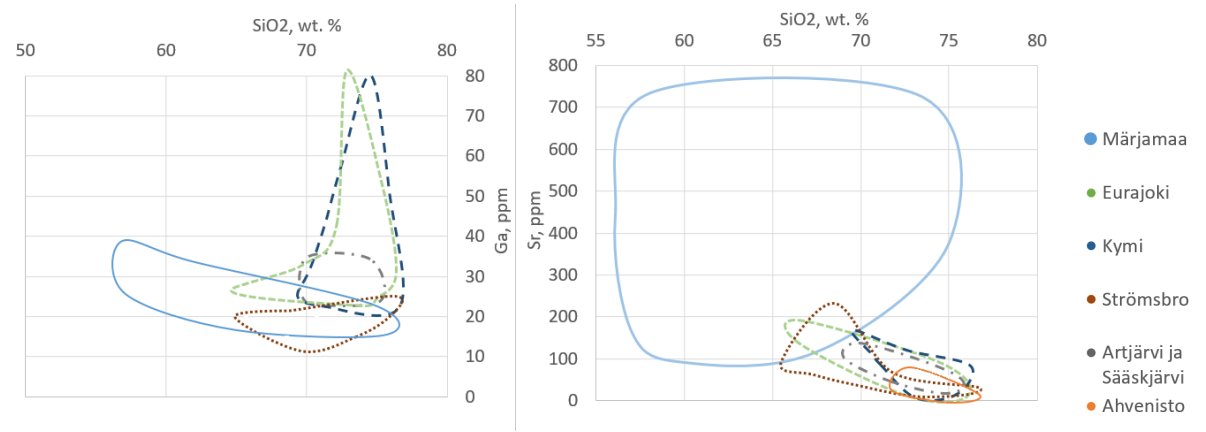

Figure 16. Geochemical composition of Svecofennian rapakivi intrusions. A) Ga is plotted against SiO_2; B) Sr is plotted against SiO_2. Analyses of Strömsbro are from Andresson (1997), Ahvenisto form Eden (1991), Artjärvi & Sääskjärvi from Lukkari (2002), Kymi from Haapala & Lukkari (2005) and Reider et al. (1996), Eurajoki from Taylor (1992) or provided by R. P. Taylor.

In Figure 16, Ga and Sr were also plotted against SiO_2. Sr seems to be in similar correlation with Rb where, Märjamaa has very low concentrations compared to other Svecofennian rapakivis apart from the Strömsbro intrusion. In addition, the Artjärvi & Sääskjärvi stock is also relatively poor in Ga. Similarly to Rb levels in Figure 15 Eurajoki and Kymi stocks have highly elevated concentrations of Ga

peaking at around 80 ppm. However, the Sr diagram in Figure 16 is similar to Zr diagram in Figure 15, where Märjamaa has highly elevated concentrations compared to other Svecofennian rapakivis, peaking at almost 800 ppm. The majority of Finnish and Swedish rapakivis stay below 150 ppm, with Eurajoki and Strömsbro reaching 200 ppm or more.

4.3. Geochronology of the Märjamaa rapakivi

Two rapakivi samples were analyzed from the Märjamaa intrusion and its Kloostri satellite. These samples were taken from cores F305 and F323. Furthermore, the U-Pb isotopic ratios of the zircons from these samples were analyzed to get an estimated age of the intrusions (Figure 17).

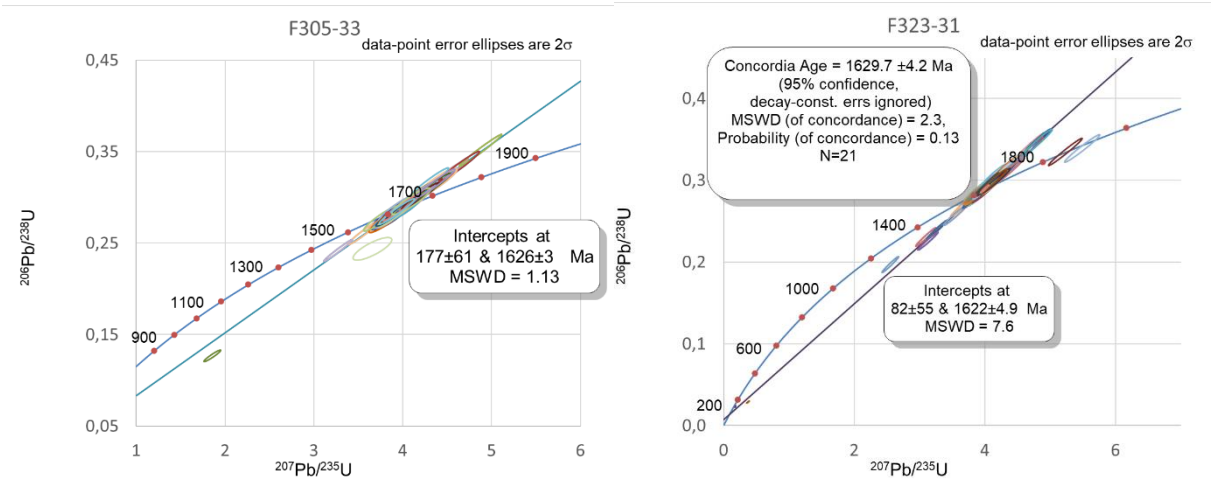

Figure 17. Results from Pb/U zircon analyses by LA-ICPMS Attom method (Laser Ablation Inductively Coupled Plasma Mass Spectrometry). Graphs are from the analyses report prepared by the Geological Survey of Finland.

Sample F305-33 zircon fractions define a discordia line with an upper intercept age of 1626 ± 3 Ma, a lower intercept age of 177 ± 61 Ma, and a MSWD (mean square of weighted deviates) of 1.13. Sample F323-31 zircon fractions define a discordia line with an upper intercept age of 1622 ± 4.9 Ma, a lower intercept age of 82 ± 55 Ma, and a MSWD of 7.6. In addition, the concordia age was also defined for sample F323-31 as 1629.7 ± 4.2 Ma with a MSWD of 2.3 and probability (of concordance) of 0.13.

5. Discussion

5.1. Geochemistry and geochronology

The porphyritic granites of the Märjamaa intrusion are similar to other Estonian rapakivis such as Neeme, Naissaare, Ereda, and Taebla. Although there is no classical rapakivi texture which includes mantled alkali feldspar ovoids among these Estonian granites, they are still categorized as A-type granites. The Märjamaa intrusion is mainly set apart from other Estonian and Fennoscandian counterparts by its variability of silica content, which can go as low as 56 wt. %. These low-silica rocks located in the center of the Märjamaa intrusion stands out due to its higher magnesium, iron, and calcium concentrations. The results support the previous characterizations about the center of the Märjamaa intrusion as being more basic (less evolved/fractionated) and highly magnetic compared to surrounding rocks (Rämö et al., 1996; Soesoo & Niin, 1992).

New data on trace elements also shows that the Märjamaa intrusion contains highly elevated levels of REEs compared to other Svecofennian rapakivi intrusions as seen in Figure 18. Unfortunately, it was not possible to compare the total REE content of Strömsbro and Ahvenisto intrusions due to the lack of trace element analyses. The average concentration of total REEs is more similar among all the intrusions compared to the high peaks. However, the average REE content is still the highest in the Märjamaa intrusion with 925 ppm, followed by the Kymi stock with 771 ppm. The lowest concentration of REEs is in the Artjärvi & Sääskjärvi, and Eurajoki stocks with 536 ppm and 415 ppm.

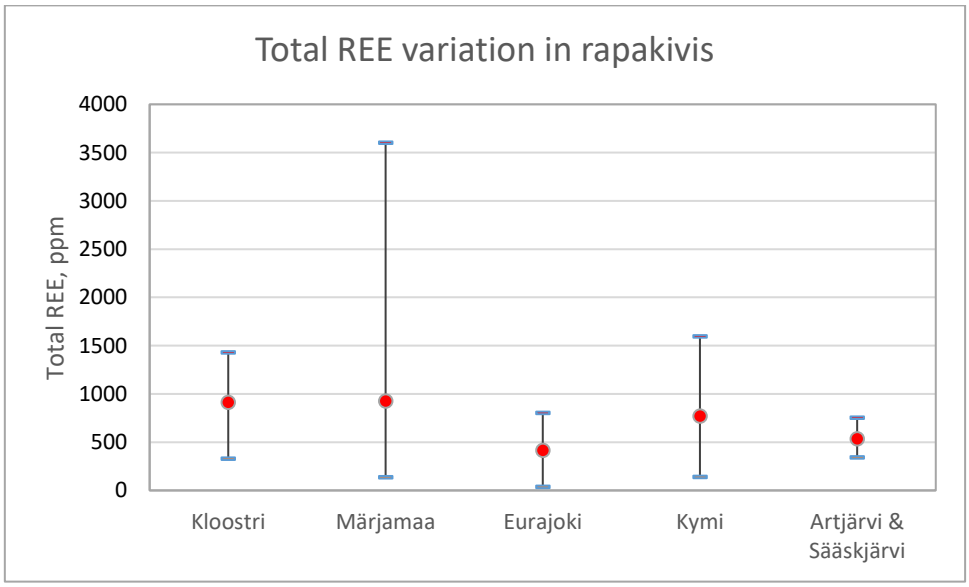

Figure 18. Total REE variation in Märjamaa intrusion and its satellite in addition to Eurajoki, Kymi, Artjärvi & Sääskjärvi intrusions. Red circles depict average and blue lines the maximum and minimum values of a stock. Analyses of Artjärvi & Sääskjärvi are from Lukkari (2002), Kymi from Haapala & Lukkari (2004) and Reider et al. (1996), Eurajoki from Taylor (1992) or provided by R. P. Taylor.

Another element that stands out in the Märjamaa intrusion is potassium, which does not have a defined trend and is relatively higher than the other Svecofennian rapakivis, especially among more mafic rocks. Furthermore, there seem to be two evolutionary trends among the Märjamaa potassium

concentrations, where one set of data points follows the usual trend of potassium content lowering among more mafic rocks. The other trend shows a slight increase in potassium with the decrease of silica concentration. This second trend can be tied to the sericitization of plagioclase, which was widely seen in Photograph 7. Haapala addressed this topic in his 1977 article, where he explained that the sericitization of plagioclase increases the potassium concentration in the rock, which he verified by electron microscopy. Potassium increase during the sericitization of plagioclase is usually followed by a decrease in sodium content. This phenomenon can also be seen in Figure 14, where the Märjamaa intrusion has much lower potassium concentrations compared to other Finnish and Swedish rapakivis.

According to Haapala (1977), Rb and Ga concentrations are also related to metasomatic processes. This happens when both the feldspar and mica have been metasomatically altered. As seen in Figures 15 & 16 Finnish and Swedish rapakivis tend to be richer in Rb and Ga due to exposure to fluids which were most likely rich in these elements. In addition, this has resulted in lower Ba and Sr concentrations. However, the opposite trend can be seen within the Märjamaa intrusion, which has very low Rb and Ga content and extremely high Ba and Sr concentrations. The Finnish and Swedish rapakivi granites might have thus been subjected to extensive metasomatism compared to the Märjamaa granites.

The Märjamaa intrusion is categorized as within-plate granites with the data slightly tilting towards volcanic arc granites according to tectno-magmatic settings classifications of granites in Figure 12D. When comparing this data to other Finnish and Swedish rapakivis the categorization stays the same, within-plate granites. However, the tilting of the data is toward syn-collisional granites. The difference in this case is also due to the Rb content in the rapakivi. The Estonian rapakivis are poor in Rb and are thus placed slightly differently in the tectonic setting diagram. The subjection to metasomatism in Finnish and Swedish rapakivis might also be reflected in a more distorted placement in this diagram.

5.2. Geochronology

The Märjamaa intrusion has previously been dated by Kirs et al. (1991), with U-Pb zircon analyses which defined the upper intercept age at 1626 ± 13 Ma (drill core unknown). Another U-Pb analysis from the Märjamaa intrusion (drill core F303) was published by Rämö et al. (1996), where the upper intercept age was defined at 1629 ± 7 Ma. Both samples were described to be taken from the main phase of the intrusion. The studied new U-Pb zircon fractions from drill core F305 define the upper intercept age of the second phase at 1626 ± 3 Ma. However, since it is unknown from which drill core the sample was taken by Kirs et al. (1991), it is difficult to compare these results spatially.

In this study the Kloostri satellite was also dated for the first time. This was done by U-Pb dating on zircon fractions from drill core F323, which is located in the core of the Kloostri sattelite. The upper intercept age was defined at 1622 ± 4.9 Ma. This result is similar to the first phase of the Märjamaa intrusion. Furthermore, this supports the hypothesis that the Kloostri satellite was formed during the third phase.

The Märjamaa intrusion and its satellite Kloostri have been categorized by age into the Wiborg suiten in which rapakivis formed between 1.65-1.62 Ga (Figure 19). This is further confirmed by the new geochronological analyses. All the Estonian intrusions (including Märjamaa, Naissaare, Neeme, Taebla and Ereda) fall into this interval in addition to the Wiborg batolith and its satellites. The Strömsbro

and Laitila intrusions are categorized by age into the Åland suiten which has a formation age interval of 1.58-.1.56 Ga.

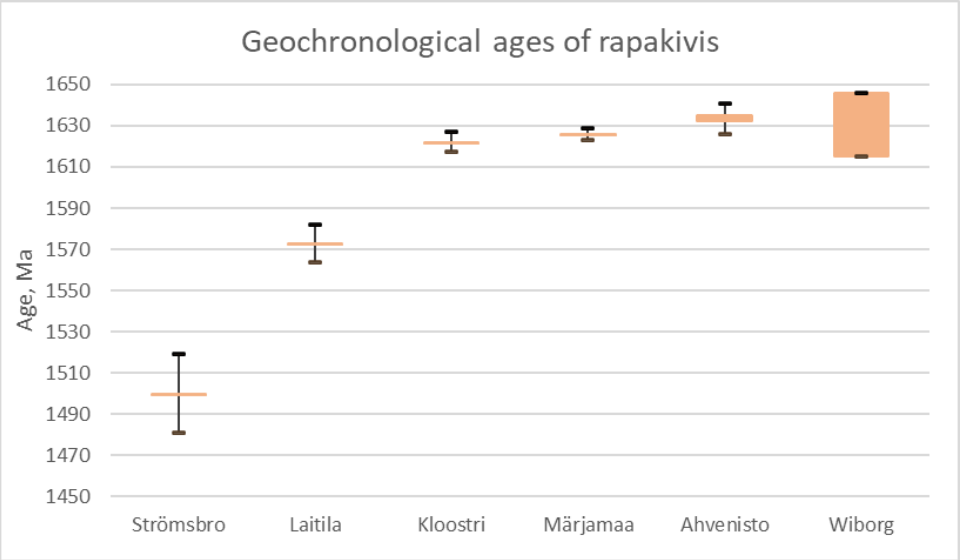

Figure 19. The geochronology of rapakivis: Strömsbro (Andresson, 1997), Laitila (Vaasjoki,, 1977), Kloostri, Märjamaa, Ahvenisto (Alviola et al., 1999), Wiborg (Vaasjoki et al., 1991).

5.3. Formation and geochemical features of the Märjamaa rapakivi intrusion

Three intrusive phases have been previously identified from the Märjamaa intrusion (Soeseoo & Niin, 1992; 1993). The main intrusive phase consists of the highly magnetic core of the Märjamaa intrusion with the second phase surrounding the core. The Kloostri satellite has been interpreted as the third and final phase of the Märjamaa intrusion formation.

However, it has also been theorized that the Kloostri granitoid might be a separate stock-like granitoid. The geochemical similarities between the main Märjamaa intrusion to the Kloostri granitoid can be seen in Figures 9 & 13. It is clear from these figures that the Kloostri granitoid and the Märjamaa second intrusive phase have very similar geochemical characteristics. In addition, the results from the geochronological analyses confirm that the Kloostri granitoid formed later than the first and second phase, with a difference in the upper intercept age of *ca* 7-4 Ma. Taking all this into account, it seems logical to assume that the Kloostri granitoid, is part of the third phase of the Märjamaa intrusion (Figure 20).

Two clear trends could be noted when plotting trace elements, including REEs against P2O5 as seen in Figure 13. The first trend includes drill cores F323, F314, and F305 and the second trend drill cores F306 and F303. These two trends depict clear differentiation between phases. However, it is interesting to see F306 and F303 following a similar trend, when the rapakivi in core F306 is usually characterized as the first and main phase of the intrusion and core F303 as part of the second phase. Soesoo (1993) categorized the rapakivi surrounding F303 as a separate subtype of granites. This area could be an interesting topic for further studies.

The first trend characterizes mostly granites from the second and third intrusive phases. However, core F305 has previously also been categorized as part of the main phase based on previous microscopy (Soesoo, 1993). In addition, the Klein et al. (1994) study placed the drill core exactly between the first and second phase. When comparing the distribution of phases from previous studies to the aeromagnetic map in the Maa-amet webpage, it seems clear that drill core F305 stands outside of the highly magnetic main phase. Using the aeromagnetic map a new layout of the main phase was drawn in Figure 20.

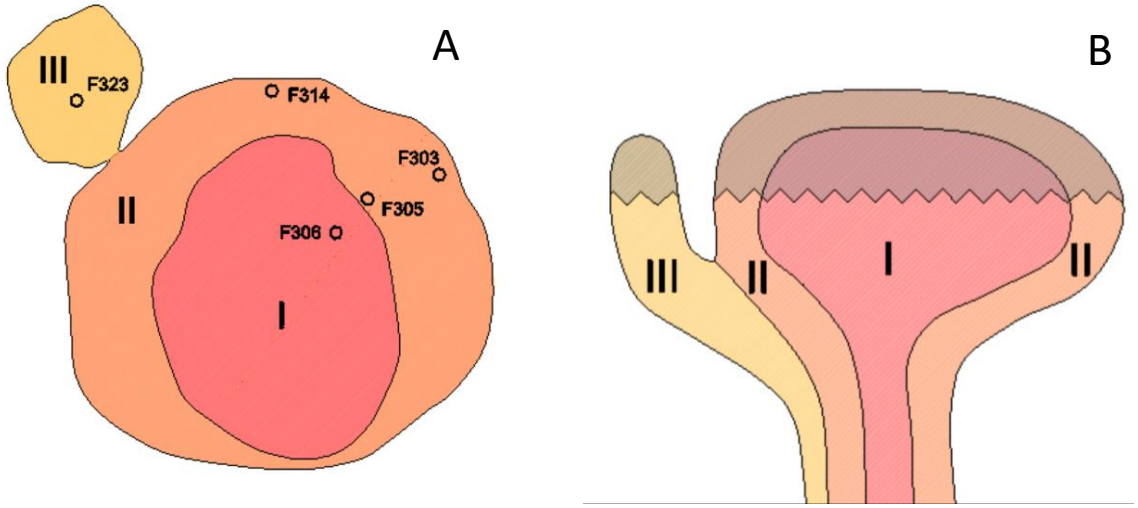

Figure 20. Outlines of magmatic intrusion phases in the Märjamaa intrusion. A) The outline of the first, second, and third phase of the Märjamaa intrusion with the locations of drill cores F303, F305, F306, F314, and F323. The outlines were drawn using the Maa-amet WMS services. B) A rough crosscut of the Märjamaa intrusion showing the first, second, and third intrusion phase. The gray area depicts the eroded part of the intrusion.

Table 3. Positive correlations of REEs in the Märjamaa rapakivi intrusion

Interval	La	Ce	Pr	Nd	Sm	Eu	Gd	Tb	Dy	Ho	Er	Tm	Yb	Lu	TOT-REE
>1400 ppm	537	1066	122	425	63	6,6	55	6,7	31	6,1	16	1,9	12	1,8	2350
900-1400 ppm	257	504	57	197	29	4,8	25	3,1	14	2,9	7,4	1,0	6,1	0,9	1110
500-900 ppm	140	288	36	134	22	3,9	19	2,5	12	2,4	6,3	0,9	5,5	0,8	673
< 500 ppm	67	130	16	59	9,7	2,8	8,3	1,1	5,4	1,1	2,9	0,4	2,6	0,4	307

Another interesting grouping occurs in Figure 11B in which P2O5 is plotted against Sr. This has resulted in the separate grouping of all drill cores. This implies that there is a unique Sr content in all drill cores,

with the concentration level in a core staying very similar throughout the intrusion despite the depth variation.

Another type of grouping was formed by ranking all analyses by their total REE content and dividing them into intervals as seen in Table 3. It turned out that all REEs, including LREEs and HREEs, were in strong positive correlation (between 0,599-0,997) to each other (Appendix 13). However, elements like Le, Ce, and Eu displayed a weaker correlation (mostly between 0,599-0,854) compared to others. The occurrence of REEs is usually related to the presence of zircon and apatite in the rock, but the occurrence of elements like Le, Ce, and Eu might also be tied to another mineral. For example, Eu could also be found in feldspar. Out of all the other trace elements Zn, Ga, Y, Zr, Nb, Mo, Cs, Hf, Ta, Tl, Th, and U were also in positive correlation with the REEs (Appendix 14). Only Mn and S were in full correlation with the REEs, while Fe, Ti, Ca, P were only partly correlated (Appendix 15). The correlation of Fe, Ti, Ca, and P to REEs may have decreased over time due to secondary processes within the intrusion. However, elements such as Rb, Sr, Ba, Si, Na, and K have no positive correlation to REEs.

A trend of high REE concentrations at similar depths was also noted throughout the Märjamaa intrusion, which can be seen in Figure 21. The interval of enriched REEEs also had a tilt which mimicked the bedrock surface. The cause of these high concentrations might be due to late-stage magmatic fractionation, where the system contained lots of fluids. This late-stage solidification probably also has a high concentration of zircon and apatite crystals which are the main carriers of REEs. This would explain the similar enrichment throughout all Märjamaa intrusive phases.

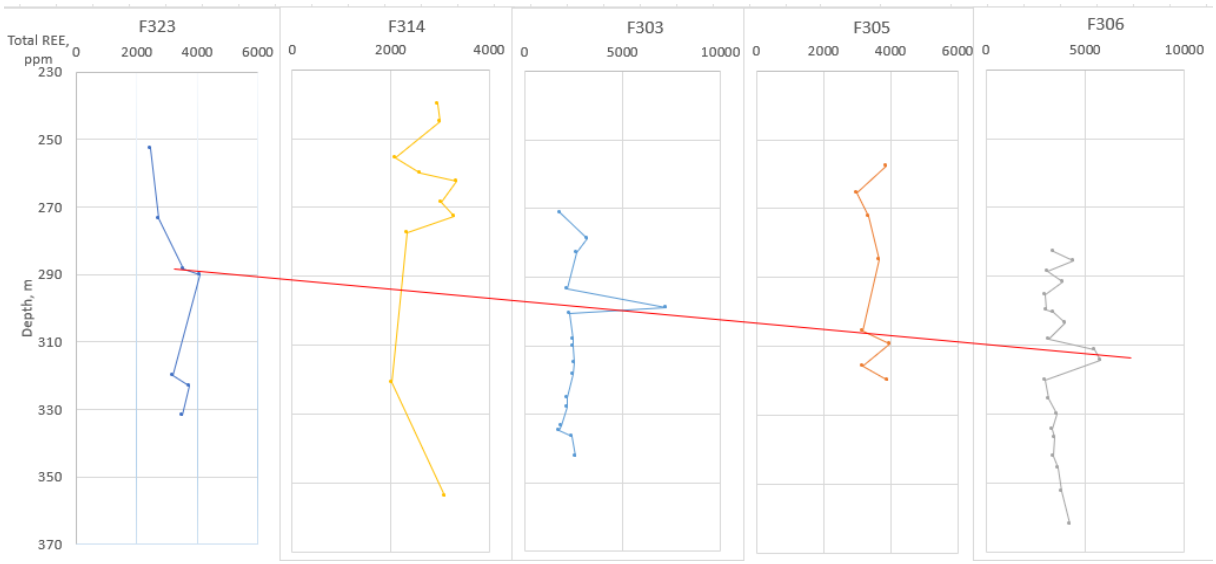

Figure 21. Total trace elements plotted against their measured depth from the ground. Each line represents a drill core, which is lined up in a direction from north to south to give an accurate representation of the bedrock surface decline.

6. Conclusions

The Märjamaa rapakivi intrusion in the northwest of Estonia is characterized as an A-type granite. The porphyry potassium granites contain quartz, microcline, plagioclase, biotite, hornblende, and muscovite with opaque minerals such as ilmenite, magnetite, pyrite, and titanite. Accessory minerals like zircon, apatite, fluorite, shpene, and orthite have also been found.

The intrusion stands out among other Svecofennian rapakivi intrusions due to its high to very high REE content reaching total values of 3600 ppm. Within the intrusion highly enriched interval of REEs was also found at a depth of 290-315 m from the ground. In addition, total REE value is in positive correlation among LREEs and HREEs alike.

The Märjamaa intrusion has been subjected to considerably less metasomatism compared to its Finnish and Swedish counterparts. This is evident in the extremely poor concentration of Rb and Ga and high concentrations of Ba and Sr. In addition, the geochemical similarities of the Märjamaa intrusion to its primary magma composition is also evident in the uncorrelated nature between elements such as Ba, Rb, and Sr. However, sericitization of plagioclase within the intrusion is common and has resulted in the slight enrichment of potassium and depletion of sodium.

The Märjamaa intrusion formed as a result of intraplate magmatism over the course of multiple intrusive phases. The main phase of the intrusion formed at 1629 ± 7 Ma, followed by the second phase of the intrusion which formed at 1626 ± 3 Ma, and the third phase including the Kloostri satellite which formed at 1622 ± 4.9 Ma.

Acknowledgements

I would like to express my sincere gratitude to my supervisors, Alvar Soesoo and Juan David Solano Acosta, for their constant guidance, patience, and valuable insight throughout the making of this thesis. Without their help, this thesis could not have been executed.

I am very grateful to the Geological Survey of Estonia for their resources and permission to get samples. I would also like to thank Kristjan Urtson for his insight in microscopy. Finally, I would like to extend my thanks to Rutt Hints for helping me find a subject for this thesis.

References

Alviola, R., Johanson, B. S., Rämö, O. T., & Vaasjoki, M. (1999). The Proterozoic Ahvenisto rapakivi granite–massif-type anorthosite complex, southeastern Finland; petrography and U–Pb chronology. *Precambrian Research, 95*(1-2), 89-107.

Andersson, U. B. (1997). The sub-Jotnian strömsbro granite complex at gävle, Sweden. *GFF, 119*(2), 159-167.

Chappell, B. W. (1974). Two Contrasting Granite Types. *Pacific Geology*, *8,* 173-174.

Clarke, D. B. (1992). *Granitoid rocks* (Vol. 7). Springer Science & Business Media.

Edén, P. (1991). A specialized topaz-bearing rapakivi granite and associated mineralized greisen in the Ahvenisto complex, SE Finland. *Bulletin of the Geological Society of Finland, 63*, 25-40.

Elo, S., & Korja, A. (1993). Geophysical interpretation of the crustal and upper mantle structure in the Wiborg rapakivi granite area, southeastern Finland. *Precambrian Research, 64*(1-4), 273-288.

Ewart, A. (1982). The mineralogy and petrology of Tertiary-Recent orogenic volcanic rocks: with special reference to the andesitic-basaltic compositional range. *Andesites: Orogenic Andesites and Related Rocks*, 26-87.

Frost, B. R., & Frost, C. D. (2008). A geochemical classification for feldspathic igneous rocks. *Journal of Petrology,* 49, 11, 1955-1969.

Haapala, I. (1977). The controls of tin and related mineralizations in the rapakivi-granite areas of south-eastern Fennoscandia. *Geologiska Föreningen i Stockholm Förhandlingar, 99*(2), 130-142.

Haapala, I., & Rämö, O. T. (1992). Tectonic setting and origin of the Proterozoic rapakivi granites of southeastern Fennoscandia. *Earth and environmental science transactions of the Royal Society of Edinburgh, 83*(1-2), 165-171.

Haapala, I. (1997). Magmatic and postmagmatic processes in tin-mineralized granites: topaz-bearing leucogranite in the Eurajoki rapakivi granite stock, *Finland. Journal of Petrology, 38*(12), 1645-1659.

Haapala, I., & Lukkari, S. (2005). Petrological and geochemical evolution of the Kymi stock, a topaz granite cupola within the Wiborg rapakivi batholith, Finland*. Lithos, 80*(1-4), 347-362.

Kirs. J. (1986). X-ray and optical investigation of feldspars from Estonian early platform potassium granites. *Acta Comment. Univ. Tartuensis, 759*, 3-19 (in Russian).

Kirs, J. H., Huhma, H., & Haapala, I. (1991). Petrological-chemical features and age of Estonian anorogenic potassium granites. In *Symposium on Rapakivi Granites and Realted Rocks, Abstract Volume* (Vol. 34, pp. 28-29). Geol. Surv. Finland.

Kirs, J. H., Haapala, I., & Rämö, O. T. (2004). Anorogenic magmatic rocks in the Estonian crystalline basement. In *Proceedings of the Estonian Academy of Sciences. Geology* (Vol. 53, No. 3, pp. 210-225).

Kivisilla, J. (1991). Geochemistry of the anorogenic porphyritic potassium granites of Estonia. In *Symposium on Rapakivi Granites and Realted Rocks, Abstract volume* (Vol. 34, pp. 30). Geol. Surv. Finland.

Kivisilla, J., Niin, M., & Koppelmaa, H. (1999). *Catalogue of chemical analyses of major elements in the rocks of the crystalline basement of Estonia*. Eesti Geoloogiakeskus.

Koistinen, T. J. (Ed.). (1994). *Precambrian basement of the Gulf of Finland and surrounding area 1:1 000 000*. Geological Survey of Finland.

Koistinen, T., Klein, V., Koppelmaa, H., Korsman, K., Lahtinen, R., Nironen, M., Puura, V., Saltikova, T., Tikhomirov, S., & Yanovskiy, A. (1996). Paleoproterozoic Svecofennian orogenic belt in the surroundings of the Gulf of Finland. *SPECIAL PAPER-GEOLOGICAL SURVEY OF FINLAND,* 21-58.

Koppelmaa, H., Gromov, O., Kivisilla, J., Klein, V., Lodjak, T., Mardla, A., Niin, M., Puura, V., & Suuroja, K. (1982). *Aruanne süvakaardistamisest Tallinn Kõrvemaa piirkonnas (Põhja-Eesti) mõõtkavas 1:500 000 1978.-1982. a.* Geoloogia Valitsus.

Korja, A., Korja, T., Luosto, U., & Heikkinen, P. (1993). Seismic and geoelectric evidence for collisional and extensional events in the Fennoscandian Shield implications for Precambrian crustal evolution. *Tectonophysics, 219*(1-3), 129-152.

Korja, A., & Heikkinen, P. J. (1995). Proterozoic extensional tectonics of the central Fennoscandian Shield: Results from the Baltic and Bothnian Echoes from the Lithosphere experiment. *Tectonics, 14*(2), 504-517.

Korja, A., Lahtinen, R., & Nironen, M. (2006). The Svecofennian orogen: a collage of microcontinents and island arcs. *Geological Society, London, Memoirs, 32*(1), 561-578.

Kuuspalu, T. (1975). Rapakivi granites of the crystalline basement of Estonia. *Acta Comment. Univ. Tartuensis, 359,* 76-141.

Lukkari, S. (2002). Petrography and geochemistry of the topaz-bearing granite stocks in Artjärvi and Sääskjärvi, western margin of the Wiborg rapakivi granite batholith. *Bulletin of the Geological Society of Finland, 74*(1-2), 115-132.

Maa-amet. (23.05.2024). 1:400 000 geoloogilised kaardid. http://www.xgis.maaamet.ee/xgis2/page/app/geoloogia400k

McDonough, W. F., & Sun, S. S. (1995). The composition of the Earth. *Chemical Geology, 120* (3-4), 223–253 .

Oen, I. S., Helmers, H., Verschure, R. H., & Wiklander, U. (1982). Ore deposition in a Proterozoic incipient rift zone environment: a tentative model for the Filipstad-Grythyttan-Hjulsjö region, Bergslagen, Sweden*. Geologische Rundschau, 71*, 182-194.

Origin Analytical. (23.05.2024). ICP-MS, ICP-OES & LA-ICP-MS. https://originanalytical.com/process/icp-ms-icp-oes/

Pearce, J. A., Harris, N. B., & Tindle, A. G. (1984). Trace element discrimination diagrams for the tectonic interpretation of granitic rocks. *Journal of petrology*, *25*(4), 956-983.

Puura, V., Vaher, R., Klein, V., Koppelmaa, H., Niin, M., Vanamb, V., & Kirs, J. (1983). The crystalline basement of Estonian territory. *(English summary). Nauka, Moscow.* 202-206 .

Puura, V., Klein, V., Koppelmaa, H., & Niin, M. (1997). Precambrian basement. *In: Raukas, A., Teedumäe, A. (ed.), Geology and mIneral Resources of Estonia.* Estonian Academy Publishers, Tallinn. 27-34 .

Puura, V., & Flodén, T. (1999). Rapakivi-granite–anorthosite magmatism—a way of thinning and stabilisation of the Svecofennian crust, Baltic Sea Basin. *Tectonophysics, 305*(1-3), 75-92.

Rieder, M., Haapala, I., & Povondra, P. (1996). Mineralogy of dark mica from the Wiborg rapakivi batholith, southeastern Finland. *European Journal of Mineralogy 8*(3), 593 – 605.

Ripa, M., & Stephens, M. B. (2020). Chapter 10 Magmatism (1.6–1.4 Ga) and Mesoproterozoic sedimentation related to intracratonic rifting coeval with distal accretionary orogenesis. *Geological Society, London, Memoirs, 50*(1), 269-288.

Rämö, O. T., & Haapala, I. (1995). One hundred years of rapakivi granite. *Mineralogy and Petrology, 52*(3), 129-185.

Rämö, O. T., Huhma, H., & Kirs, J. (1996). Radiogenic isotopes of the Estonian and Latvian rapakivi granite suites: new data from the concealed Precambrian of the East European Craton. *Precambrian Research, 79* (3-4), 209-226.

Sederholm, J. J. (1891) Über die finnländischen Rapakiwigesteine. *Tschermak's Mineral. Petrogr. Mitth., 12,* 1-31.

Simonen, A., & Vorma, A. (1969). *Amphibole and biotite from rapakivi.* Geologinen tutkimuslaitos.

Soesoo, A., & Niin, M. (1992). Petrographical and petrochemical features of the Estonian Precambrian porphyraceous potassium granites. In *Proceedings of the Estonian Academy of Science, Geology* (Vol. 41, No. 3, pp. 93-107).

Soesoo, A. (1993). Estonian porphyraceous potassium granites: petrochemical subdivision and petrogenetical interpretation. *Proceedings of the Estonian Academy of Sciences, Geology* (Vol. 42, No. 3, pp. 97-109).

Soesoo, A., Puura, V., Kirs, J., Petersell, V., Niin, M., & All, T. (2004). Outlines of the Precambrian basement of Estonia. *Proceedings of the Estonian Academy of Sciences, Geology* (Vol. 53, No. 3, pp. 149-164).

Soesoo, A., Nirgi, S., & Plado, J. (2020). The evolution of the Estonian Precambrian basement: geological, geophysical, and geochronological constraints. *Proceedings of the Kaerlian Research Centre of the Russian Academy of Sciences, (2),* 18-33.

Skridlaite, G., Bogdanova, S., Taran, L., & Baginski, B. (2014). Recurrent high grade metamorphism recording a 300 Ma long Proterozoic crustal evolution in the western part of the East European Craton. *Gondwana Research, 25*(2), 649-667.

Taylor, R. (1992). Petrological and geochemical characteristics of the Pleasant Ridge zinnwaldite-topaz granite, southern New Brunswick, and comparisons with other topaz-bearing felsic rocks. *Canadian Mineralogist, 30*, 895-921.

Vaasjoki, M. (1977). Rapakivi granites and other postorogenic rocks in Finland: their age and the lead isotopic composition of certain associated galena mineralizations. *Geological Survey of Finland, Bulletin, (294), 1-71.*

Vaasjoki, M., & Rämö, T. (1989). *The Wiborg rapakivi batolith and associated rocks in South-Eastern Finland: Excursion A2 (Vol. 30).* Geologian tutkimuskeskus, Geologiska forskiningscentralen.

Vaasjoki, M., Rämö, O. T., & Sakko, M. (1991). New U-Pb ages from the Wiborg rapakivi area: constraints on the temporal evolution of the rapakivi granite-anorthosite-diabase dyke association of southeastern Finland. *Precambrian Research, 51*(1-4), 227-243.

Van Achterbergh, E., Ryan C., Jackson, S., & Griffin, W. (2001). Data reduction software for LA-ICP-MS, in: Laser-Ablation ICPMS in the Earth Sciences – Principles and applications. *Mineralogical Association of Canada short course series, 29*, 239-243.

Van der Velden, W., Baker, J., de Maesschalck, S., & van Meerten, T. (1982). Bimodal early Proterozoic volcanism in the Grythytte field and associated volcano-plutonic complexes, Bergslagen, Central Sweden. *Geologische Rundschau, 71*, 171-181.

Vigneresse, J. L. (2005). The specific case of the Mid-Proterozoic rapakivi granites and associated suite within the context of the Columbia supercontinent. *Precambrian research, 137*(1-2), 1-34.

Vorma, A. (1971). On the contact aureole of the Wiborg rapakivi granite massif in southwestern Finland. *Geological Survey of Finland, Bulletin, 255.*

Vorma, A. (1976). On the petrochemistry of rapakivi granites with special reference to the Laitila massif, southwestern Finland. *Geological Survey of Finland, Bulletin, 285.*

Whalen, J. B., Currie, K. L., & Chappell, B. W. (1987). A-type granites: geochemical characteristics, discrimination and petrogenesis. *Contributions to mineralogy and petrology, 95*(4), 407-419.

Appendix

Appendix 1. Description of dill core F306 – Käbi. Translated from (Koppelmaa et al., 1982).

In drillhole F306, basement rocks lie at a depth of 271 m.

The first 9,4 m (271.0-280.4 m) consist of strongly weathered porphyritic potassium granite which has kaolinized in the beginning of the rock.

The next interval is 9,6 m long (280.4-290.0 m). The degree of weathering is less significant with weathering decreasing in this interval. The rock consists of reddish-pink porpyritic plagiomicrocline granite with scattered dissemination of magnetite.

The weathering crust ends at a depth of 290.0 m and from there continues unaltered porphyritic plagimicrocline granite which stays homogeneous up to a depth of 358.0 m. The sizes of prismatic microcline phenocrystals in the rock are generally up to 2x3 cm, with some reaching up to 4x6 cm. Their arragement is sporadic and does not have a single orientation, comprising 30-70% of the whole rock. The colour of these phenochrystals is pinkish. The dimentions of plagioclase inclusions do not exceed 1x2 mm.

The bulk of the granite is composed mainly of quartz, microcline, plagioclase, and dark-colored minerals, such as mainly biotite and to a lesser extent hornblende and magnetite. The sizes of these darker minerals range from 1x2 to 5x8 mm. Slight dissemination of pyrite is also observed.

In the last interval, 358.5-363.0, porphyritic plagiomicrocline granite becomes slightly more leucocratic and the number and size of phenocrystals increases.

Appendix 2. Description of drill core F314. Translated from (Koppelmaa et al., 1982).

In drillhole F314 basement rocks lie at a depth of 229.9 m.

The first 8.0 m (229.9-237.9 m) consists of strongly weathered reddish gray medium grained migmatized biotite-amphibolite gneisses which have a banded texture and white spots of kaolinite.

This is followed by 1.1 m (237.9-239.0) of weathered red porphyritic granites with a massive texture and white kaolinite spots.

The next interval is 9.5 m long (239.0-248,5 m). It consists of homogeneous porphyritic red coarse granites with microcline phenocrystals, biotite and amphibole (Marjamaa granite).

Interval 248.5-254.0 m contains migmatized medium grained biotite-amphibolite gneisses with ortho- and clinopyroxenes. It has a banded texture and is dark gray with a greenish tint.

Interval 254.0-255.6 m alternates to fine grained leucocratic red granites which has a massive texture.

The next interval is 17.2 m long (255.6-274.0 m). Homogeneous red coarse-grained granites containing microcline phenocrysts, biotite and amphibolite with massive texture. In interval 273.4-274.0 m dissemination of magnetite is observed.

From 274.0-278.2 m. Medium-grained migmatized biotite-amphibolite gneisses with clinopyrocene. The gneisses are banded and are gark gray with a greenish tint.

From 278.2-281.0 m. Red pegmatoid plagiomicrocline granites with a massive texture and accumulations of chloritized biotite.

From 281.0-283.8 m. Medium-grained migmatized biotite-amphibolite gneisses with pyroxene. The gneisses are finely banded and are dark grey with a greenish tint.

From 283.8-287.4 m. Red granites on biotite-amphibole gneiss, medium grained.

From 287.4-289.5 m Medium-grained migmatized biotite-amphibolite gneisses with compact texture. The gneisses are dark grey with a greenish tint.

From 289.5-291.3 m. Fine-grained leucocratic red granites with massive texture.

From 291.3-292.1 m. Medium-grained migmatized biotite-amphibole gneisses with thin bands . The gneisses are dark grey with a greenish tint.

From 292.1-298.1 m. Medium to coarse-grained amphibolites with clinopyroxene. The rock is dark green, weakly migmatized, with an unclear fine texture.

From 298.1-310.0 m. Medium-grained migmatized biotite-amphibole gneisses with pyroxene. Rock is unclearly banded and is dark gray with a greenish tint. At depths of 301.7 and 307.0 m dissemination of magnetite occurs and at a depth of 303.7 m sulfides occur.

From 310.0-311.3 m. Medium-grained dark green melanocratic biotite amphibolites.

From 311.3-322.7 m. Medium-grained migmatized biotite-amphibole gneisses with pyroxene. The gneisses are clearly banded and are dark grey with greenish or reddish tints. At depths 312.5,314.0,320.0,321.0 m disseminated magnetism occurs.

From 322.7-328.0 m. Migmatized medium-grained biotite-amphibole gneisses with an unclear banded texture. Colour is reddish gray with a greenish tint.

From 328.0-328.8 m. Granites on biotite-amphibole gneisses.

From 328.8-338.6 m. Weakly migmatized and migmatized biotite-amphibole gneisses with ortho- and clinopyroxenes. The gneisses are banded and dark coloured with a greenish tint.

From 338.6-339.6 m. Medium grained granites on biotite-amphibole gneisses. The colour is grayish red.

From 339.8-347.0 m. Weakly migmatized and migmatized biotite-amphibolite gneisses with pyroxene, dark grey with a greenish tint, unclearly banded.

From 347.0-349.0 m. Migmatites on biotite-amphibole gneisses.

From 349.0-352.8 m. Medium –grained migmatized biotite-amphibole gneiss with pyroxene. Rock has a banded texture and is reddish-gray.

From 352.8-355.0 m. Red medium to coarse-grained plagiomicrocline granite with massive texture.

From 355.0-358.2 m. Red plagiomicrocline pegmatoid granite with massive texture. At a depth of 355.4-356.8 quartz vein.

From 358.2-359.8 m. Migmatized medium-grained biotite-amphibole gneisses with unclear banding.
From 359.8-360.3 m. Plagiomicrocline pegmatitic granite.

From 360.3-361.0 m. Migmatized biotite-amphibole geniss.

Appendix 3. Chrondrite normalized diagram of trace elements within drill core F303. Normalization after McDonough & Sun (1995).

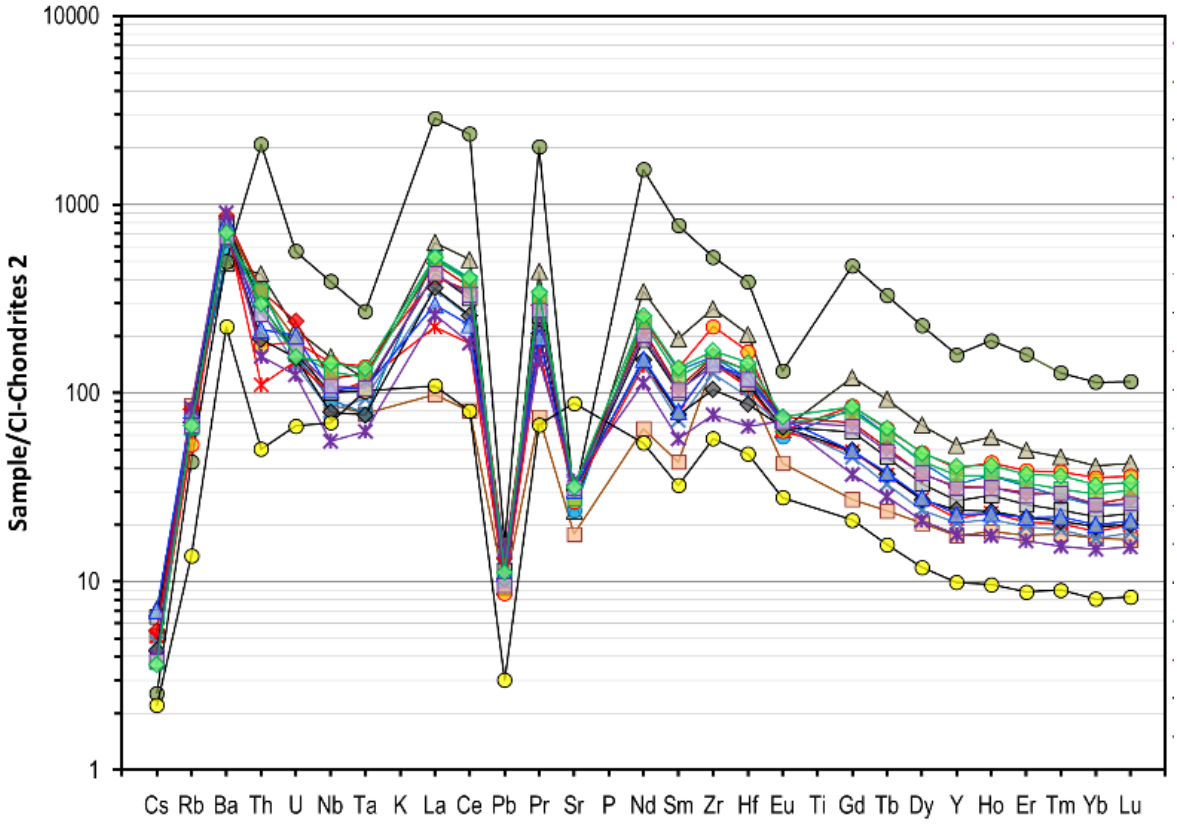

Appendix 4. Chondrite normalized diagram of REEs within drill core F303. Normalization after McDonough & Sun (1995).

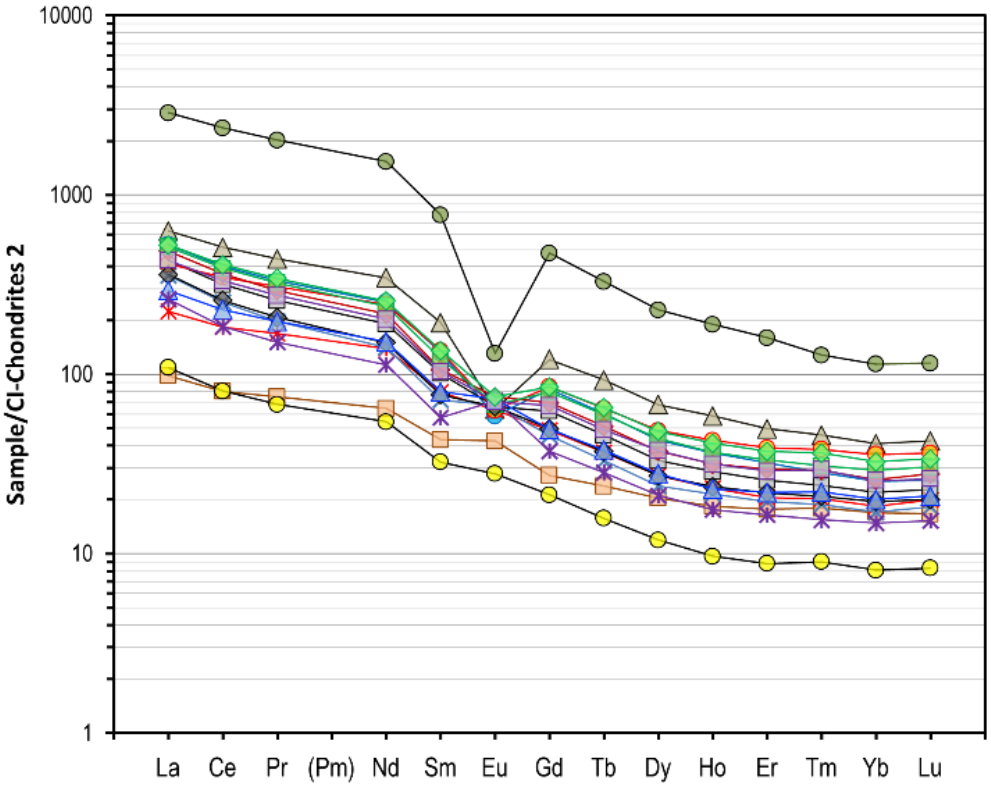

Appendix 5. Chondrite normalized diagram of trace elements within drill core F305. Normalization after McDonough & Sun (1995).

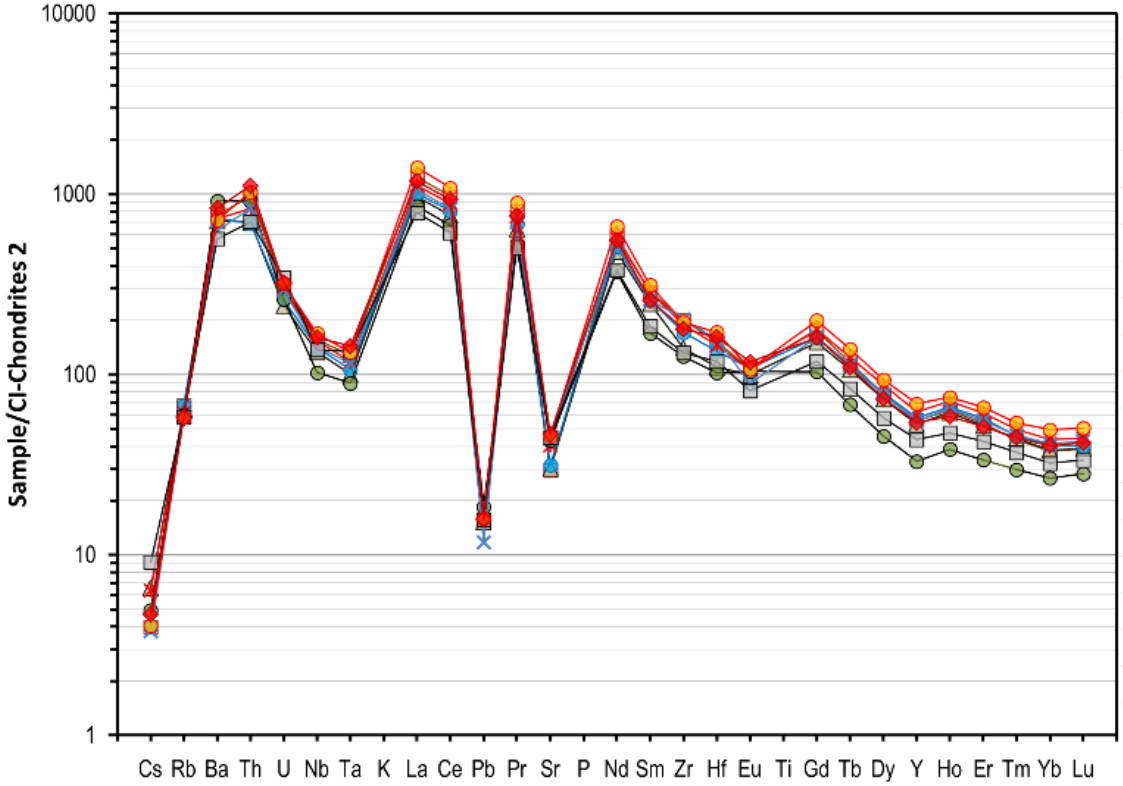

Appendix 6. Chondrite normalized diagram of REEs within drill core F305. Normalization after McDonough & Sun (1995).

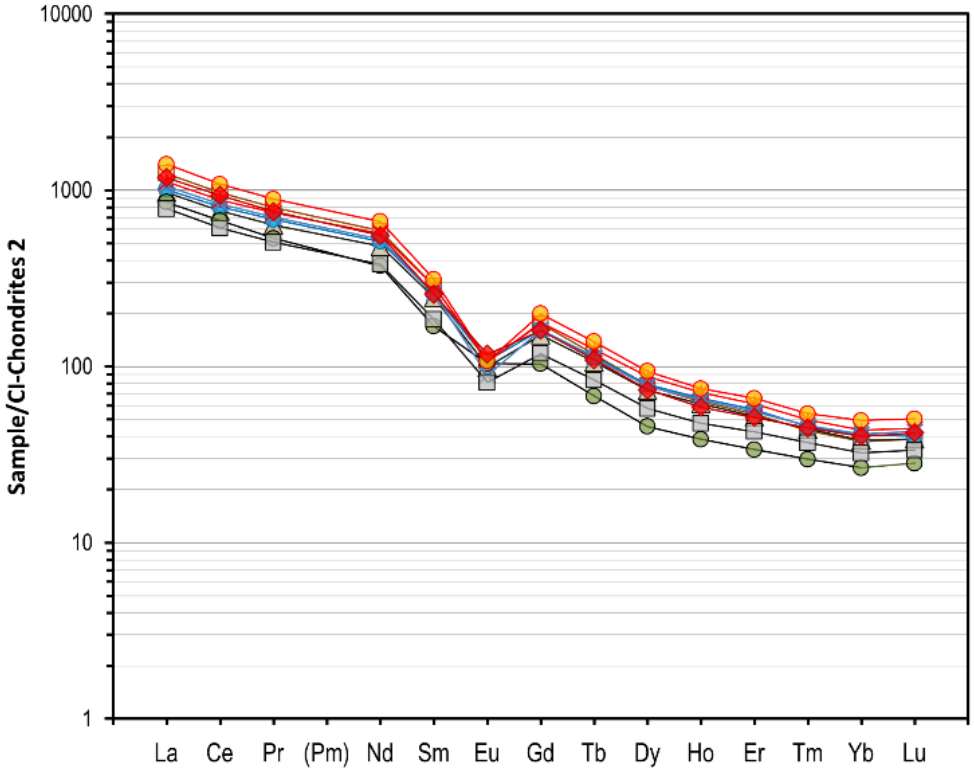

Appendix 7. Chondrite normalized diagram of trace elements within dill core F306. Normalization after McDonough & Sun (1995).

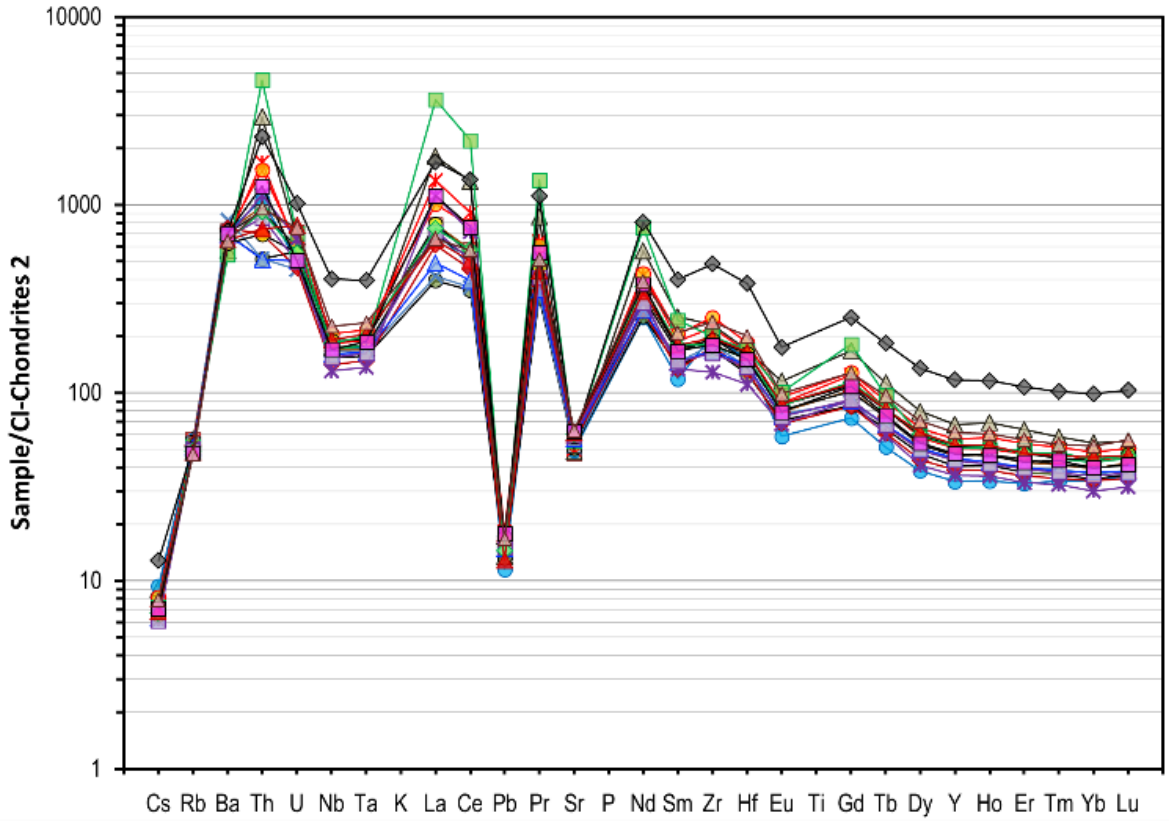

Appendix 8. Chondrite normalized diagram of REEs within drill core F306. Normalization after McDonough & Sun (1995).

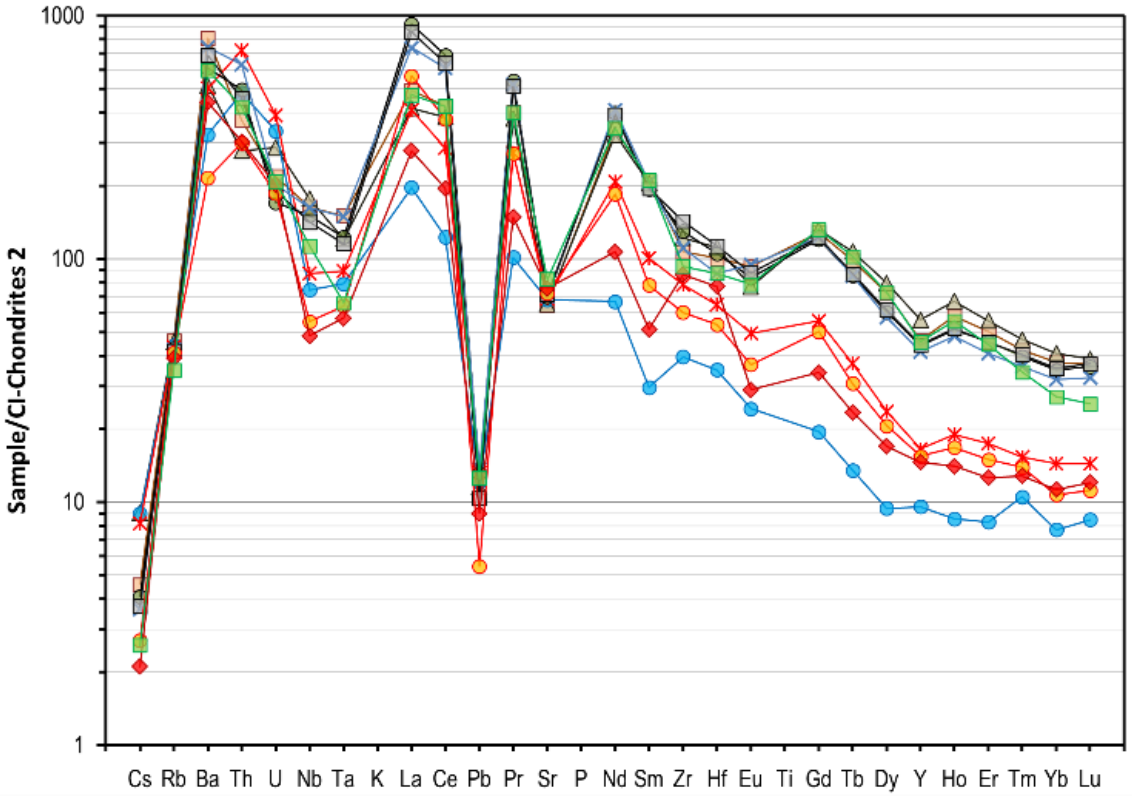

Appendix 9. Chondrite normalized diagram of trace elements within drill core F314. Normalization after McDonough & Sun (1995).

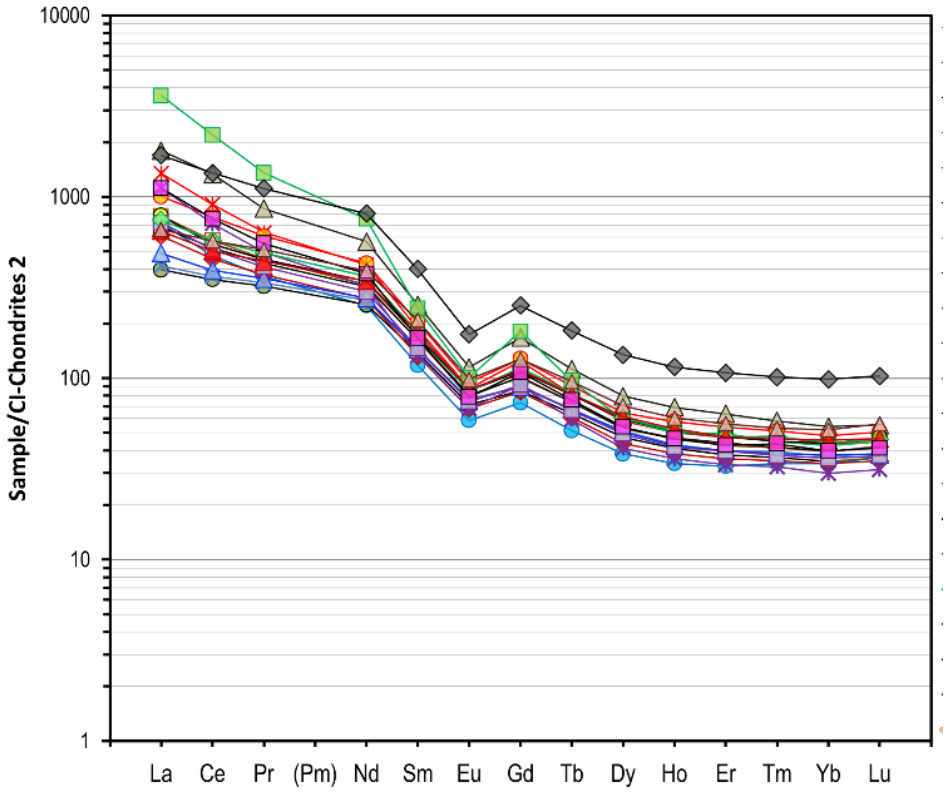

Appendix 10. Chondrite normalized diagram of REEs within drill core F314. Normalization after McDonough & Sun (1995).

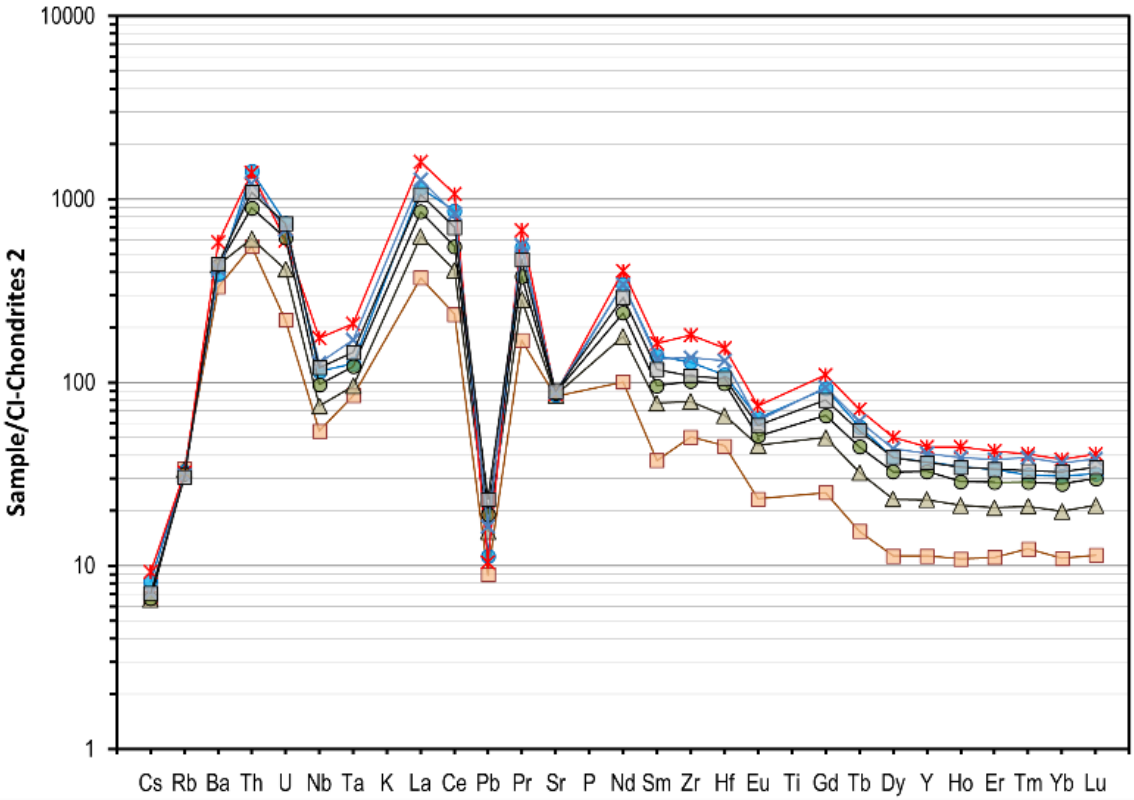

Appendix 11. Chondrite normalized diagram of trace elements within drill core 323. Normalization after McDonough & Sun (1995).

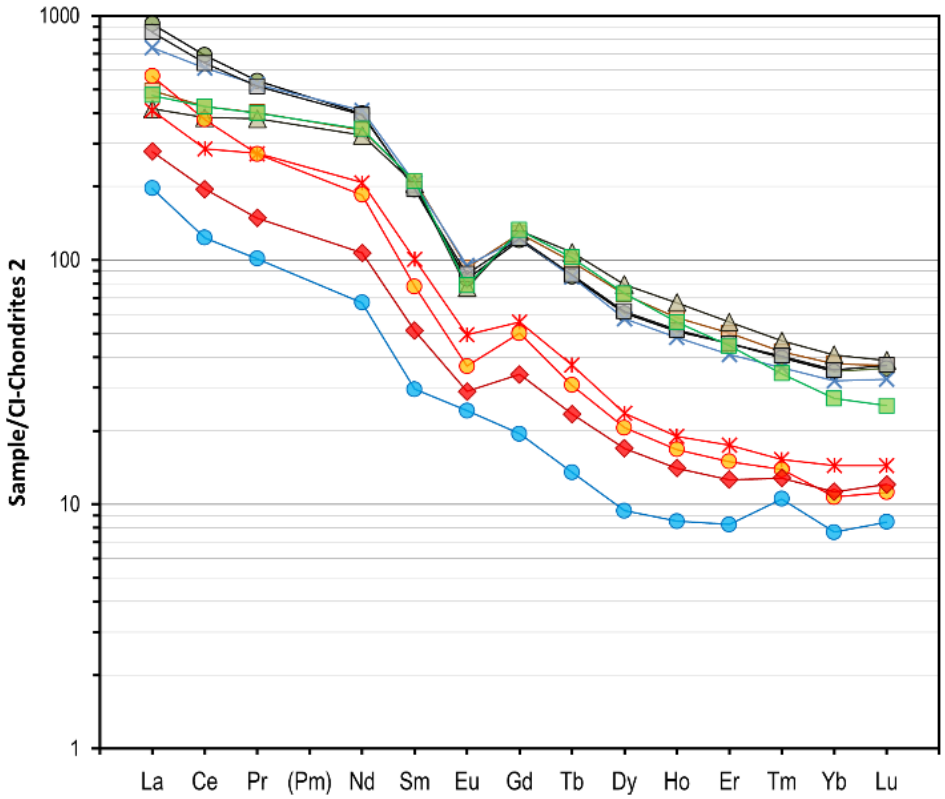

Appendix 12. Chondrite normalized diagram of REEs within drill core F323. Normalization after McDonough & Sun (1995).

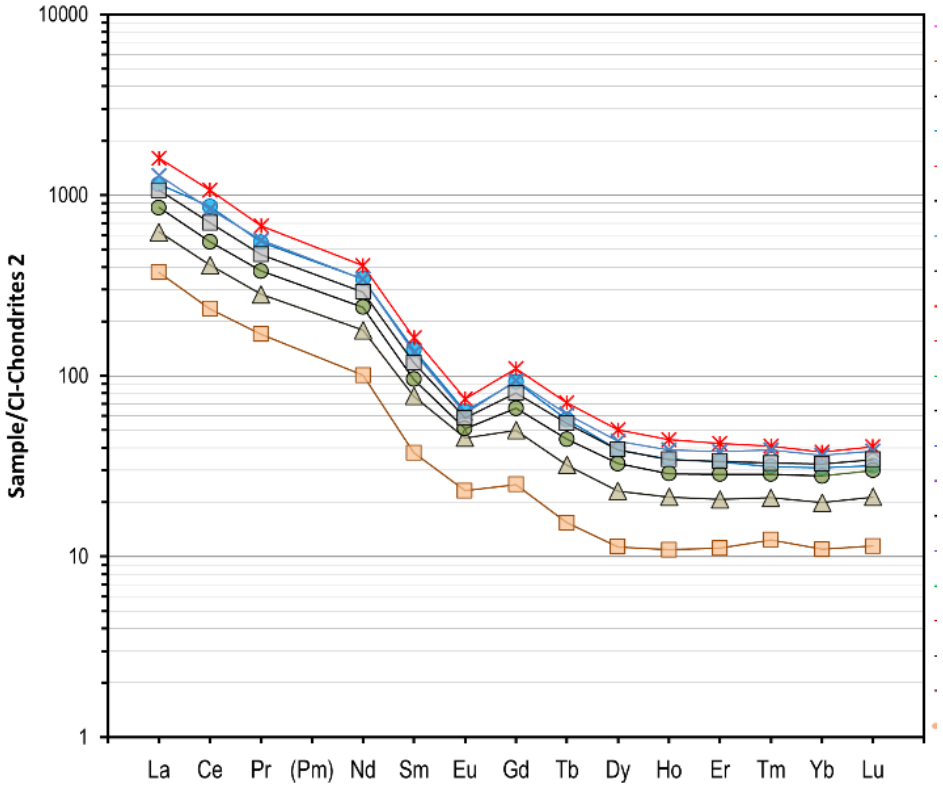

Appendix 13. Correlation matrix between REEs.

	La	*Ce*	*Pr*	*Nd*	*Sm*	*Eu*	*Gd*	*Tb*	*Dy*	*Ho*	*Er*	*Tm*	*Yb*	*Lu*
La	1													
Ce	0,982	1												
Pr	0,919	0,975	1											
Nd	0,835	0,920	0,984	1										
Sm	0,702	0,818	0,923	0,976	1									
Eu	0,599	0,689	0,758	0,790	0,796	1								
Gd	0,749	0,854	0,946	0,987	0,997	0,800	1							
Tb	0,669	0,789	0,900	0,960	0,996	0,802	0,992	1						
Dy	0,634	0,759	0,876	0,943	0,988	0,803	0,982	0,997	1					
Ho	0,642	0,765	0,878	0,942	0,984	0,803	0,980	0,994	0,998	1				
Er	0,673	0,789	0,892	0,945	0,976	0,820	0,975	0,986	0,991	0,996	1			
Tm	0,674	0,780	0,871	0,914	0,936	0,825	0,939	0,950	0,961	0,972	0,987	1		
Yb	0,673	0,773	0,856	0,892	0,907	0,822	0,912	0,921	0,934	0,949	0,971	0,995	1	
Lu	0,678	0,773	0,851	0,883	0,892	0,820	0,898	0,906	0,918	0,935	0,961	0,990	0,998	1

Appendix 14. Major and trace element correlation matrix.

	TiO_2	*Fe_2O_3*	*MnO*	*Sc*	*Zn*	*Ga*	*Rb*	*Sr*	*Y*	*Zr*	*Nb*	*Ba*	*Total REE*
TiO_2	1												
Fe_2O_3	0,885	1											
MnO	0,767	0,837	1										
Sc	0,895	0,911	0,806	1									
Zn	0,791	0,887	0,854	0,892	1								
Ga	0,710	0,809	0,742	0,781	0,850	1							
Rb	0,037	0,046	-0,048	0,061	-0,003	0,085	1						
Sr	-0,181	-0,264	-0,108	-0,256	-0,205	-0,257	-0,908	1					
Y	0,664	0,780	0,760	0,836	0,918	0,805	-0,040	-0,163	1				
Zr	0,829	0,877	0,777	0,919	0,908	0,778	0,158	-0,352	0,888	1			
Nb	0,795	0,799	0,774	0,878	0,895	0,773	-0,067	-0,096	0,929	0,907	1		
Ba	0,107	0,039	0,093	0,144	0,130	0,237	0,694	-0,616	0,124	0,222	0,179	1	
Total REE	0,490	0,601	0,640	0,678	0,757	0,763	-0,139	-0,031	0,850	0,715	0,747	-0,013	1

Appendix 15. Major and trace element correlation matrix.

	SiO_2	TiO_2	Fe_2O_3	MgO	CaO	Na_2O	K_2O	P_2O_5	Zr	Nb	Nd	Total REE
SiO_2	1											
TiO_2	-0,758	1										
Fe_2O_3	-0,809	0,885	1									
MgO	-0,731	0,785	0,667	1								
CaO	-0,746	0,722	0,717	0,713	1							
Na_2O	-0,330	0,175	0,170	0,356	0,584	1						
K_2O	0,375	-0,416	-0,392	-0,589	-0,772	-0,723	1					
P_2O_5	-0,696	0,935	0,760	0,808	0,687	0,130	-0,378	1				
Zr	-0,630	0,829	0,877	0,428	0,532	-0,065	-0,174	0,703	1			
Nb	-0,488	0,795	0,799	0,406	0,444	-0,075	-0,180	0,696	0,907	1		
Nd	-0,318	0,500	0,665	0,160	0,345	-0,031	-0,156	0,358	0,778	0,808	1	
Total REE	-0,286	0,490	0,601	0,215	0,317	-0,013	-0,156	0,386	0,715	0,747	0,958	1

Lisa
rektori 07.04.2020 käskkirjale nr 1-8/17

Lihtlitsents lõputöö reprodutseerimiseks ja lõputöö üldsusele kättesaadavaks tegemiseks[1]

Mina Carina Potagin

1. Annan Tallinna Tehnikaülikoolile tasuta loa (lihtlitsentsi) enda loodud teose
Geology, geochemistry, and geochronology of the Märjamaa rapakivi granite intrusion

mille juhendaja on Alvar Soesoo,

1.1 reprodutseerimiseks lõputöö säilitamise ja elektroonse avaldamise eesmärgil, sh Tallinna Tehnikaülikooli raamatukogu digikogusse lisamise eesmärgil kuni autoriõiguse kehtivuse tähtaja lõppemiseni;

1.2 üldsusele kättesaadavaks tegemiseks Tallinna Tehnikaülikooli veebikeskkonna kaudu, sealhulgas Tallinna Tehnikaülikooli raamatukogu digikogu kaudu kuni autoriõiguse kehtivuse tähtaja lõppemiseni.

2. Olen teadlik, et käesoleva lihtlitsentsi punktis 1 nimetatud õigused jäävad alles ka autorile.

3. Kinnitan, et lihtlitsentsi andmisega ei rikuta teiste isikute intellektuaalomandi ega isikuandmete kaitse seadusest ning muudest õigusaktidest tulenevaid õigusi.

27.05.2024

(allkirjastatud digitaalselt)

[1] *Lihtlitsents ei kehti juurdepääsupiirangu kehtivuse ajal vastavalt üliõpilase taotlusele lõputööle juurdepääsupiirangu kehtestamiseks, mis on allkirjastatud teaduskonna dekaani poolt, välja arvatud ülikooli õigus lõputööd reprodutseerida üksnes säilitamise eesmärgil. Kui lõputöö on loonud kaks või enam isikut oma ühise loomingulise tegevusega ning lõputöö kaas- või ühisautor(id) ei ole andnud lõputööd kaitsvale üliõpilasele kindlaksmääratud tähtajaks nõusolekut lõputöö reprodutseerimiseks ja avalikustamiseks vastavalt lihtlitsentsi punktidele 1.1. jq 1.2, siis lihtlitsents nimetatud tähtaja jooksul ei kehti.*